

Dr. Andreas Richter

Co-Editor

Atmospheric Chemistry and Physics

Oct. 20, 2019

Dear Dr. Richter,

Subject: Revision and resubmission of manuscript #acp-2019-472

Thanks again for your careful reviewing of our manuscript and your suggestions. We have carefully reviewed the comments and have revised the manuscript accordingly. Our responses are given in a point-by-point manner below. In addition, Jianfeng Li has moved to PNNL, and the affiliation was updated.

We tracked all the changes and updated the reference format following the ACP style. And we hope the revised version is now suitable for publication.

Please address all correspondence concerning this manuscript to Dr. Yuhang Wang (yuhang.wang@eas.gatech.edu).

Thanks again for your time.

Sincerely,

Jianfeng Li

School of Earth and Atmospheric Sciences

Georgia Institute of Technology

311 Ferst Drive

Atlanta, GA, 30332-0340

Response to Co-editor

Thank you for a careful and thorough reading of the manuscript and for your thoughtful comments and suggestions. Our answers follow the Co-editor's comments (in *Italics*).

Comments / Suggestions:

• In my opinion, a weakness of this work is the lack of separation between chemical and other factors resulting in non-linearities. In the manuscript, chemical non-linearities are often mentioned but they probably play only a minor role compared to the main factor, the relative contribution of anthropogenic to total NO_x emissions in a given grid cell. If that's possible, it would therefore be good to add some information on which fraction of the observed non-linearity is really due to chemical non-linearities.

Reply:

Thank you for your suggestions. As we mentioned before, it is tough to accurately quantitatively separate the contributions of each factor to β and γ values due to their complex interactions during the 3-D model. Here, we qualitatively estimated the chemical nonlinearity by using the chemical lifetime of NO_x. We updated Figure S7 in the revised supplement figure file, comparing the chemical lifetimes of NO_x for the standard REAM simulation (“group 1” in Section 3.1 in the main manuscript) and those for the model results from “group 2” with reduced anthropogenic NO_x emissions. Since the NO_x chemical lifetimes change little, we can state that chemical nonlinearity does not contribute significantly to the nonlinear relationships in low-anthropogenic-NO_x emission regions where background sources and transport strongly affect β and γ values.

In high-anthropogenic-NO_x emission regions, the impact of background sources and transport effects on β and γ values is much weaker than that in low-anthropogenic-NO_x emission regions; therefore, lifetime change should be taken into consideration for more careful analyses but not for this study due to the sharp contrast between rural and urban regions.

Although Figure S7 indeed gives the relative changes of NO_x chemical lifetimes, the relative changes of chemical lifetimes are not directly related to $\frac{\Delta\Omega}{\Omega}$ and $\frac{\Delta c}{c}$ in Equations (1) and (2) in the main manuscript. The following gives a simple example.

We assume that NO_x emission E_0 is emitted at time 0, and the chemical lifetime of NO_x is τ . The decay of E_0 against chemistry is described below.

$$\begin{aligned}\frac{dE}{dt} &= -\frac{1}{\tau}E \\ E &= E_0 e^{-\frac{1}{\tau}t}\end{aligned}\tag{1}$$

For another chemical lifetime of NO_x, assuming $\tau_1 = 1.1 \times \tau$, we have

$$\begin{aligned}E_1 &= E_0 e^{-\frac{1}{\tau_1}t} \\ \frac{E}{E_1} &= e^{t\left(\frac{1}{\tau_1} - \frac{1}{\tau}\right)} = e^{t\left(\frac{\tau - \tau_1}{\tau_1 \tau}\right)} = e^{\frac{-1}{11\tau}t}.\end{aligned}\tag{2}$$

Therefore, the ratio of E to E_1 is not only related to τ but also related to t , both nonlinear. In our 3-D model, it will be much more complex, as τ is changing in different

hours, and other processes are involved. Equation (2) provides some qualitative information:

$$\begin{aligned} \tau > \tau_1, \quad \frac{E}{E_1} > 1 \\ \tau < \tau_1, \quad \frac{E}{E_1} < 1 \end{aligned} \quad . \quad (3)$$

If we reduce E_0 by 15%, and the chemical lifetime is τ' .

$$\begin{aligned} E' &= 0.85E_0 e^{-\frac{1}{\tau'}t} \\ \frac{E-E'}{E} &= \frac{E_0 e^{-\frac{1}{\tau}t} - 0.85E_0 e^{-\frac{1}{\tau'}t}}{E_0 e^{-\frac{1}{\tau}t}} = 1 - 0.85e^{t\left(\frac{\tau'-\tau}{\tau\tau'}\right)} \\ \text{if } \tau' < \tau & \\ \frac{E-E'}{E} &> 1 - 0.85 = 0.15 \\ \frac{0.15}{\frac{E-E'}{E}} &< 1 \end{aligned} \quad (4)$$

This is why β and γ values are < 1 at 13:00 – 14:00 when the chemical lifetimes of NO_x in bin #9 in Figure S7 decrease due to decreased anthropogenic NO_x emissions.

Now we assume $\tau' = 0.9\tau$,

$$\begin{aligned} \frac{E-E'}{E} &= 1 - 0.85e^{t\left(\frac{\tau'-\tau}{\tau\tau'}\right)} = 1 - 0.85e^{-t\frac{1}{\tau}} \\ 0.15 &< \frac{E-E'}{E} < 1 \end{aligned} \quad (5)$$

The left-hand term $\frac{E - E'}{E}$ is negatively correlated to τ . With a larger τ , we will have a smaller left-hand term, and then larger β and γ values. So here, we qualitatively explained your last question: why that β and γ at 13:00 – 14:00 are smaller than those at 10:00 – 11:00 reflects strong chemical nonlinearity at noon than in the morning? The chemical lifetime of NO_x at noontime is shorter than in the morning. More NO_x is oxidized due to stronger chemistry, and less NO_2 is left as surface concentrations or NO_2 TVCDs — this is what we called chemical nonlinearity.

We corrected some errors and made some modifications in Lines 238 – 239 and 254 – 265 to make it more consistent with Figure S7. To take into consideration the accumulation of NO_x emissions (several hours of chemical lifetimes) against chemistry, we used the chemical lifetimes at 8:00 – 11:00 and at 11:00 – 14:00, which we think more accurately represent the responses of NO_2 TVCD and NO_2 surface concentrations to NO_x emissions due to chemical nonlinearity.

- *Abstract, line 17: “non-linearity in the emission-TVCD relationship” should be “anthropogenic emission”*

Reply:

Thanks. We corrected it. Please see Line 18 in the revised manuscript.

- *Introduction, line 31: “unfavourable to climate change” – please rephrase*

Reply:

Thanks. We changed “which are unfavorable to human health, ecosystem stabilities, and climate change” to “, all of which have negative environmental impacts”. Please see Lines 31 - 33 in the revised manuscript.

• *Introduction, line 35: now soil emissions are mentioned specifically making the statement more correct but highlighting that these numbers without an estimate for lightning NO_x are incomplete. Please add an estimate for lightning.*

Reply:

We added the estimated lightning NO_x emissions over the US in 2014 from the GEOS-Chem model results. Please see Lines 36 – 39 in the revised manuscript.

• *Line 64: paragraph starts with chemical non-linearities, suggesting that the following discussion is about chemistry while I would argue that most of the following observations are explained by the relative contribution of anthropogenic emissions, not chemical non-linearities.*

Reply:

Thank you for your suggestion. We changed “the nonlinearity in NO_x chemistry” to “their nonlinear dependences on anthropogenic NO_x emissions”. Please see Lines 67 – 68 in the revised manuscript.

• *Line 84: again, chemical non-linearity is mentioned explicitly but I find this misleading.*

Reply:

Thanks. We added background sources and physical processes in the sentence. Please see Line 87 in the revised manuscript.

- *Line 204: “in part” – are there any other possible reasons for the non-linearity?*

Reply:

Biomass burning is another NO_x source, but its emissions are low and can be neglected over the CONUS compared to lightning and soil NO_x (EPA, 2018; Silvern et al., 2019). Also, biomass burning is mainly in rural regions, and its effects are limited over urban regions in the long term, although severe wildfires may affect urban regions in some specific conditions. Since we used “background sources” in Lines 207 – 208 and biomass burning emissions are also NO_x background sources, we deleted “in part” in Line 207 in the revised manuscript. Also, we added NO₂ hydrolysis on aerosols but deleted NO₂ wet deposition in Lines 207 – 208. REAM doesn’t consider the direct wet deposition of NO₂. Therefore, we also updated the sentences in Lines 238 – 239 in the revised manuscript and Lines 68 and 174 in the revised supplement figure file.

- *Line 251: I can’t really see the difference in variability between the two overpass times...*

Reply:

In Lines 254 – 257 in the revised manuscript, we mean the standard deviations of β and γ values in the same bins. We changed the sentence to make it clearer. We listed their

standard deviations in the following table, clearly showing larger standard deviations at 10:00 – 11:00 LT than 13:00 – 14:00 LT except for β values for bin #1 and bin #8. It is noteworthy that only 1 grid cell belongs to bin #9.

Table 1. Uncertainties of β and γ values during different periods for each anthropogenic-NO_x-emission bin in Figure 2 in the main manuscript

| | β | | γ | |
|---------------------|---------------|---------------|---------------|---------------|
| | 10:00 - 11:00 | 13:00 - 14:00 | 10:00 - 11:00 | 13:00 - 14:00 |
| bin #1 ¹ | 17.06 | 18.23 | 15.08 | 14.32 |
| bin #2 | 7.53 | 3.49 | 5.48 | 1.90 |
| bin #3 | 4.83 | 1.84 | 3.64 | 1.09 |
| bin #4 | 3.55 | 1.05 | 1.77 | 0.48 |
| bin #5 | 0.72 | 0.54 | 0.46 | 0.28 |
| bin #6 | 0.62 | 0.31 | 0.37 | 0.19 |
| bin #7 | 0.35 | 0.28 | 0.27 | 0.18 |
| bin #8 | 0.13 | 0.15 | 0.11 | 0.08 |
| bin #9 | 0.00 | 0.00 | 0.00 | 0.00 |

¹ bin #1 denotes $E \in (0, 2^1)$, bin #2 denotes $E \in [2^1, 2^2)$, etc.

As mentioned above, it is hard to quantitatively separate their contributions to β and γ values due to the interactions among transport, chemistry, aerosol uptake of NO₂, and NO₂ dry deposition. However, we can make our estimates indirectly. We have shown that the chemical lifetimes of NO_x change little, the uncertainties of the lifetime relative changes are small, and chemical nonlinearity is not a big issue in low-anthropogenic-NO_x emission regions (Figure S7). NO₂ hydrolysis on aerosols and dry deposition are proportional to NO₂ concentrations which are determined by transport and chemistry. The lifetimes of NO_x against NO₂ hydrolysis and dry deposition are almost the same for

“group 1” and “group 2” simulation results. That is to say, transport is the most critical factor in non-emission factors (excluding background sources) in low-anthropogenic- NO_x emission regions. As the uncertainties of β_{Emis} at 10:00 – 11:00 LT are close to those at 13:00 – 14:00 LT (their relative differences are $< 15\%$), and the uncertainties of γ_{Emis} are the same for 10:00 – 11:00 and 13:00 – 14:00 LT, the differences of the standard deviations of β (γ) values at 10:00 – 11:00 from those at 13:00 – 14:00 are mainly from non-emission factors — that is transport dominated in low-anthropogenic- NO_x emission regions.

• *Line 256: ... and even if it were present, why is that indicative of chemical non-linearity?*

Reply:

Please see the answer to the first question. Also, in Figure S7, (g) and (h) shows that the relative changes of NO_x chemical lifetime at noontime are even larger than those in the morning, again causing β and γ values at noontime smaller than in the morning.

References

Air Pollutant Emissions Trends Data: <https://www.epa.gov/air-emissions-inventories/air-pollutant-emissions-trends-data>, 2018.

Silvern, R. F., Jacob, D. J., Mickley, L. J., Sulprizio, M. P., Travis, K. R., Marais, E. A., Cohen, R. C., Laughner, J. L., Choi, S., Joiner, J., and Lamsal, L. N.: Using satellite observations of tropospheric NO_2 columns to infer long-term trends in US NO_x emissions: the importance of accounting for the free tropospheric NO_2 background, *Atmos. Chem. Phys.*, 19, 8863-8878, <https://doi.org/10.5194/acp-19-8863-2019>, 2019.

Inferring the anthropogenic NO_x emission trend over the United States during 2003 - 2017 from satellite observations: Was there a flattening of the emission trend after the Great Recession?

Jianfeng Li^{1,a}, Yuhang Wang^{1*}

¹ School of Earth and Atmospheric Sciences, Georgia Institute of Technology, Atlanta, Georgia, USA

^a [Now at Pacific Northwest National Laboratory, Richland, WA, USA](#)

* *Correspondence to* Yuhang Wang (yuhang.wang@eas.gatech.edu)

Abstract

We illustrate the nonlinear relationships among anthropogenic NO_x emissions, NO_2 tropospheric vertical column densities (TVCDs), and NO_2 surface concentrations using model simulations for July 2011 over the contiguous United States (CONUS). The variations of NO_2 surface concentrations and TVCDs are generally consistent and reflect well anthropogenic NO_x emission variations for high-anthropogenic- NO_x emission regions. For low-anthropogenic- NO_x emission regions, however, nonlinearity in the [anthropogenic](#) emission-TVCD relationship due to emissions from lightning and soils, chemistry, and physical processes makes it difficult to use satellite observations to infer anthropogenic NO_x emission changes. The analysis is extended to 2003 – 2017. Similar variations of NO_2 surface measurements and coincident satellite NO_2 TVCDs over urban regions are in sharp contrast to the large variation differences between surface and satellite observations over rural regions. We find a continuous decrease of anthropogenic NO_x emissions after 2011 by examining surface and satellite measurements in CONUS urban regions, but the decreasing rate is lower by 9% - 46% than the pre-2011 period.

1. Introduction

Anthropogenic emissions of nitrogen oxides ($\text{NO}_x = \text{NO}_2 + \text{NO}$) adversely affect the environment, not only because of their direct detrimental impacts on human health (Greenberg et al., 2016; Greenberg et al., 2017; Heinrich et al., 2013; Weinmayr et al., 2009), but also their fundamental roles in the formation of ozone, acid rain, and fine particles, all of which have negative environmental impacts ~~which are unfavorable to human health, ecosystem stabilities, and climate change~~ (Crouse et al., 2015; Kampa and Castanas, 2008; Myhre et al., 2013; Pandey et al., 2005; Singh and Agrawal, 2007). About $48.8 \text{ Tg N yr}^{-1}$ of NO_x are emitted globally from both anthropogenic (77%) and natural (23%) sources, such as fossil fuel combustion, biomass and biofuel burning, soil bacteria, and lightning (Seinfeld and Pandis, 2016). 3.85 Tg N ~~and~~ 0.24 Tg N , and 0.66 Tg N of anthropogenic ~~and~~ soil, and lightning NO_x , respectively, were emitted from the U.S. in 2014 on the basis of the 2014 National Emission Inventory (NEI2014) and the GEOS-Chem model simulations (Silvern et al., 2019); vehicle sources and fuel combustions accounted for 93% of the total anthropogenic NO_x emissions (EPA, 2017).

The U.S. anthropogenic NO_x emissions during the 2010s declined dramatically compared to the mid-2000s (EPA, 2018; Xing et al., 2013) due to stricter air quality regulations and emission control technology improvements, such as the phase-in of Tier II vehicles during 2004 – 2009 and the switch of power plants from coal to natural gas (De Gouw et al., 2014; McDonald et al., 2018). The overall reduction (about 30% - 50%) of anthropogenic NO_x emissions from the mid-2000s to the 2010s was corroborated by observed decreasing of vehicle NO_x emission factors, NO_2 surface concentrations, nitrate wet deposition flux (Figure S1), and NO_2 tropospheric vertical column densities (TVCDs) (Bishop and Stedman, 2015; Georgoulias et al., 2019; Li et al., 2018; McDonald et al., 2018; Miyazaki et al., 2017; Russell et al., 2012; Tong et al., 2015). However, the detailed NO_x emission changes after the Great Recession (from December 2007 to

June 2009) are highly uncertain. On the one hand, the U.S. Environmental Protection Agency (EPA) estimated that the Great Recession had a slight impact on the anthropogenic NO_x emission trend, and the anthropogenic NO_x emissions decreased steadily from 2002 to 2017 (Figure S2), although the emission decrease rate slowed down by about 20% after 2010 (-5.8% yr⁻¹ for 2002 – 2010, and -4.7% yr⁻¹ for 2010 – 2017, Table 1) (EPA, 2018). Fuel-based emission estimates in Los Angeles also showed a steady decrease of anthropogenic NO_x emissions after 2000 and a small impact of the Great Recession on anthropogenic NO_x emission decrease trend (Hassler et al., 2016). The continuous decrease of anthropogenic NO_x emissions was consistent with the ongoing reduction of vehicle emissions (McDonald et al., 2018). On the other hand, Miyazaki et al. (2017) and Jiang et al. (2018) found that the U.S. NO_x emissions derived from satellite NO₂ TVCDs, including OMI (the Ozone Monitoring Instrument), SCIAMACHY (SCanning Imaging Absorption SpectroMeter for Atmospheric CHartography), and GOME-2A (Global Ozone Monitoring Experiment – 2 onboard METOP-A), were almost flat from 2010 - 2015 and suggested that the decrease of NO_x emissions was only significant before 2010, which was completely different from the bottom-up and fuel-based emission estimates.

A complicating factor in inferring anthropogenic NO_x emission trends from the observations of NO₂ surface concentrations and satellite NO₂ TVCDs is their nonlinearity dependences on anthropogenic NO_x emissions in NO_x chemistry (Gu et al., 2013; Gu et al., 2016; Lamsal et al., 2011). Although the decrease rates of both NO₂ surface concentrations and coincident OMI NO₂ TVCDs slowed down after the Great Recession over the United States, Tong et al. (2015), Lamsal et al. (2015) and Jiang et al. (2018) found that the slowdown of the decrease rates derived from NO₂ surface concentrations is 12% - 79% less than those of NO₂ TVCDs (Table 1). Secondly, the slowdown of the decrease rates of NO₂ surface concentrations and OMI TVCDs over cities and power plants (Russell et al., 2012; Tong et al., 2015) is significantly less than those over the whole contiguous United States (CONUS) (Jiang et al., 2018; Lamsal et al., 2015). Moreover,

Zhang et al. (2018) found that filtering out lightning-affected measurements could significantly improve the comparison of NO₂ surface concentration and OMI NO₂ TVCD trends over the CONUS.

In this study, we carefully investigate the relationships among anthropogenic NO_x emissions, NO₂ surface concentrations, and NO₂ TVCDs over the CONUS and evaluate the impact of the relationships on inferring anthropogenic NO_x emission changes and trends from surface and satellite observations. Section 2 describes the model and datasets used in this study, including the Regional chemistry and transport Model (REAM), the EPA Air Quality System (AQS) NO₂ surface observations, and NO₂ TVCD products from OMI, GOME-2A, GOME-2B (GOME2 onboard METOP-B), and SCIAMACHY. In Section 3, we examine the nonlinear relationships among anthropogenic NO_x emissions, NO₂ surface concentrations, and NO₂ TVCDs using model simulations. Accounting for the effects of [background sources, physical processes, and](#) chemical nonlinearity, we then investigate the anthropogenic NO_x emission trends and changes from 2003 – 2017 over the CONUS. Finally, section 4 gives a summary of the study.

2. Model and Data Description

2.1 REAM

The REAM model has been applied and evaluated in many research applications including ozone simulation and forecast, emission inversion and evaluations, and mechanistic studies of chemical and physical processes (Alkuwari et al., 2013; Cheng et al., 2017; Cheng et al., 2018; Choi et al., 2008a; Choi et al., 2008b; Gu et al., 2013; Gu et al., 2014; Koo et al., 2012; Liu et al., 2012; Liu et al., 2014; Wang et al., 2007; Yang et al., 2011; Zhang et al., 2017; Zhang et al., 2018; Zhang and Wang, 2016; Zhao and Wang, 2009; Zhao et al., 2009a; Zhao et al., 2010). REAM used in this work, the model domain of which is shown in Figure 3, has 30 vertical layers

in the troposphere, and the horizontal resolution is $36 \times 36 \text{ km}^2$. The model is driven by meteorology fields from a Weather and Research Forecasting (WRF, version 3.6) model simulation initialized and constrained by the NCEP coupled forecast system model version 2 (CFSv2) products (Saha et al., 2011). The chemistry mechanism is based on GEOS-Chem v11.01 with updated reaction rates and aerosol uptake of isoprene nitrates (Fisher et al., 2016). Chemistry boundary conditions and initializations are from a GEOS-Chem ($2^\circ \times 2.5^\circ$) simulation. Hourly anthropogenic emissions on weekdays are based on the 2011 National Emission Inventory (NEI2011), while weekend anthropogenic emissions are set to be two-thirds of the weekday emissions (Beirle et al., 2003; Choi et al., 2012). Biogenic VOC emissions are estimated using the Model of Emissions of Gases and Aerosols from Nature (MEGAN) v2.10 (Guenther et al., 2012). NO_x emissions from soils are based on the Yienger and Levy (YL) scheme (Li et al., 2019; Yienger and Levy, 1995). The cloud-to-ground (CG) lightning flashes are calculated following Choi et al. (2005) and Zhao et al. (2009a) with the parameterization of CG flash rate as a function of convective mass fluxes and convective available potential energy (CAPE). The ratios of intra-cloud (IC) lightning flashes to CG flashes are parameterized as a function of the height between the freezing layer and the cloud top (Luo et al., 2017; Price and Rind, 1992). In this study, 250 moles of NO are emitted per CG or IC flash (Zhao et al., 2009a). As a result, on weekdays in July 2011, REAM has mean anthropogenic NO_x emissions of $7.4 \times 10^{10} \text{ molecules cm}^{-2} \text{ s}^{-1}$, mean soil NO_x emissions of $1.2 \times 10^{10} \text{ molecules cm}^{-2} \text{ s}^{-1}$, and mean lightning NO_x emissions of $3.4 \times 10^{10} \text{ molecules cm}^{-2} \text{ s}^{-1}$ over the CONUS.

2.2 Satellite NO_2 TVCDs

In this study, we use NO_2 TVCD products from four satellite sensors in the past decade, including SCIAMACHY, GOME-2A, GOME-2B, and OMI, the spectrometers onboard sun-synchronous satellites to monitor atmospheric trace gases. The SCIAMACHY instrument onboard the Environmental Satellite (ENVISAT) has an equator overpass time of 10:00 Local

time (LT) and a nadir pixel resolution of $60 \times 30 \text{ km}^2$. The GOME-2 instruments on Metop-A (named as GOME-2A) and Metop-B (GOME-2B) satellites cross the equator at 9:30 LT and have a nadir resolution of $80 \times 40 \text{ km}^2$. After July 15, 2013, the nadir resolution of GOME-2A became $40 \times 40 \text{ km}^2$ with a smaller scanning swath. The OMI onboard the EOS-Aura satellite has a nadir resolution of $24 \times 13 \text{ km}^2$ and overpasses the equator around 13:45 LT. More detailed information about these instruments is summarized in Table S1. These instruments measure backscattered solar radiation from the atmosphere in the ultraviolet and visible wavelength. The radiation measurements in the wavelength of 402 - 465 nm are then used to retrieve NO_2 VCDs. The retrieval process consists of three steps: 1) converting radiation observations to NO_2 slant column densities (SCDs) by using the Differential Optical Absorption Spectroscopy (DOAS) spectral fitting method; 2) separating tropospheric SCDs and stratospheric SCDs from the total NO_2 SCDs; 3) dividing the NO_2 tropospheric SCDs by the tropospheric air mass factors (AMF) to compute VCDs.

The product archives we use in this study include GOME-2B (TM4NO2A v2.3), SCIAMACHY (QA4ECV v1.1), GOME-2A (QA4ECV v1.1), OMI (QA4ECV v1.1, hereafter referred to as OMI-QA4ECV), OMNO2 (SPv3, hereafter referred to as OMI-NASA), and the Berkeley High-Resolution NO_2 products (v3.0B, hereafter referred to as OMI-BEHR). OMI-BEHR uses the tropospheric SCDs from OMI-NASA products but updates some inputs for the tropospheric AMF calculation (Laughner et al., 2018). These product archives have been previously validated (Boersma et al., 2018; Drosoglou et al., 2017; Drosoglou et al., 2018; Krotkov et al., 2017; Laughner et al., 2018; Wang et al., 2017; Zara et al., 2018). Generally, the pixel-size uncertainties of these products are $> 30\%$ over polluted regions under clear-sky conditions. We summarize the basic information about these products in Table S2. To keep the high quality and sampling consistency of NO_2 TVCD datasets, we chose pixel-size NO_2 TVCD data using the criteria listed in Table S3. After the selection, we re-gridded the pixel-size data into

the REAM 36×36 km² grid cells and calculate the seasonal means of each grid cell with corresponding daily values on weekdays (winter: January, February, and December; spring: March, April, and May; summer: June, July, and Autumn; autumn: September, October, and November). We excluded weekend data in this study to minimize the impacts of weekend NO_x emission reduction, leading to different NO₂ TVCDs between weekdays and weekends (Figure S3).

Satellite TVCD measurements can show large variations and apparent discontinuities due in part to the effects of cloud, lightning NO_x, the shift of satellite pixel coverage, and retrieval uncertainties (Figure S3; e.g., (Boersma et al., 2018; Zhang et al., 2018)). However, continuous and consistent measurements are required for reliable trend analyses. In addition to the criteria of data selection in Table S3, we compute the seasonal relative 90th percentile confidence interval, defined as $RCI = (X(95^{th} \text{ percentile}) - X(5^{th} \text{ percentile})) / \text{mean}(X)$, where X is the daily NO₂ TVCD for a given season. To compute the seasonal trend, we require that RCI is < 50% for the selected season every year in the analysis period (Table S3). About 45% of data are removed as a result.

2.3 Surface NO₂ measurements

Hourly surface NO₂ measurements from 2003 - 2017 are from the EPA AQS monitoring network (archived on <https://www.epa.gov/outdoor-air-quality-data>). Most AQS monitoring sites use the Federal Reference Method (FRM) — gas-phase chemiluminescence to measure NO₂. Few sites use the Federal Equivalent Method (FEM) – photolytic-chemiluminescence or the Cavity Attenuated Phase Shift Spectroscopy (CAPS) method. FRM and FEM are indirect methods, in which NO₂ is first converted to NO and then NO is measured through chemiluminescence measurement of NO₂* produced by NO + O₃. The difference is that FRM uses heated reducers/catalysts for the conversion of NO₂ to NO and FEM uses photolysis of NO₂ to NO. The

conversion to NO in the FRM instruments is not specific to NO₂, and non-NO_x active nitrogen compounds (NO_z) can also be reduced by the catalysts, which would cause high biases of NO₂ measurements, while the FEM method is sensitive to the photolysis conversion efficiency of NO₂ to NO (Beaver et al., 2012; Beaver et al., 2013; Lamsal et al., 2015). The CAPS method directly determines NO₂ concentrations based on a NO₂-induced phase shift measured by a photodetector. The CAPS instrument operates at a wavelength of about 450 nm and may overestimate NO₂ concentrations due to absorption of other molecules at the same wavelength (Beaver et al., 2012; Beaver et al., 2013; Keabian et al., 2005).

Due to the different characteristics of the above three methods and demonstrated biases between the FRM and the FEM by Lamsal et al. (2015), we firstly investigate the measurement discrepancies among the above three methods. There are three sites having FRM and FEM measurements simultaneously during some periods from 2013 - 2014, two sites having both FRM and CAPS data during some periods from 2015 – 2016, and one site using all three measurement methods during some periods in 2015. Figure S4 shows the hourly averaged ratios of FEM and CAPS to FRM data, respectively, for 4 seasons during 2013 – 2016. The CAPS/FRM ratios are in the range of 0.94 – 1.06 and the FEM/FRM ratios of 0.86 – 1.11. Furthermore, Zhang et al. (2018) discussed that the relative trends are not affected by scaling the observation data. As in the work by Zhang et al. (2018), we analyze the relative trends in the surface NO₂ data. We, therefore, did not scale the FRM data. At sites with FEM or CAPS measurements, we use these measurements in place of FRM data. If both FEM and CAPS data are available, we use the averages of the two datasets.

Since NO₂ surface concentrations have significant diurnal variations (Figure S5), we choose the data at 9:00-10:00 LT for comparison with GOME-2A/2B data, 10:00-11:00 LT for comparison with SCIAMACHY data, and 13:00-14:00 LT for OMI data. The seasonal *RCI* < 50% requirement is also used here to be consistent with the analysis of satellite TVCD data, and

thus about 1.5% of the data are removed. We also require that the measurement site must have valid measurements in the aforementioned 3 hours for at least one season from 2003 – 2017. The locations of the 179 selected sites using the site selection criteria are shown in Figure 1. The region definitions follow the U.S. Census Bureau (https://www2.census.gov/geo/pdfs/maps-data/maps/reference/us_regdiv.pdf).

3. Results and Discussions

3.1 Nonlinear relationships among anthropogenic NO_x emissions, NO₂ surface concentrations, and NO₂ TVCDs

NO₂ surface concentrations and NO₂ TVCD are not linearly correlated with NO_x emissions due ~~in part~~ to chemical nonlinearity, NO₂ hydrolysis on aerosols ($NO_2 \xrightarrow{\text{aerosol, } H_2O} 0.5HNO_3 + 0.5HNO_2$), ~~wet and~~ dry depositions, transport effects, and background sources (Gu et al., 2013; Lamsal et al., 2011). Therefore, it is necessary to first investigate the nonlinearities among NO_x emissions, NO₂ surface concentrations, and TVCDs over the CONUS before we compare the trends between NO₂ surface concentrations and TVCDs. The nonlinearity between NO_x emission and NO₂ TVCD is analyzed by examining the local sensitivity of NO₂ TVCD to NO_x emissions (Gu et al., 2013; Lamsal et al., 2011; Tong et al., 2015), which is defined as β in Equation (1). We further define γ as the sensitivity of NO₂ surface concentration to NO_x emission:

$$\frac{\Delta E}{E} = \beta \frac{\Delta \Omega}{\Omega} \quad (1)$$

$$\frac{\Delta E}{E} = \gamma \frac{\Delta c}{c} \quad (2)$$

where E denotes NO_x emission and ΔE denotes the change of NO_x emission; Ω denotes NO₂ TVCD, c denotes surface NO₂ concentration, and $\Delta \Omega$ and Δc denote the corresponding changes.

We computed β and γ values for July 2011 over the CONUS using REAM. To compute local β and γ values, we added another independent group of chemistry species (“group 2”) in REAM in order to compute the standard and sensitivity simulations concurrently. The original chemical species in the model (“group 1”) were used in the standard simulation. For group 2 chemical species, anthropogenic NO_x emissions were reduced by 15%. In the model simulation, we first computed the advection of group 1 tracers. The horizontal tracer fluxes were therefore available. All influxes into a grid cell for group 2 tracer simulation were from group 1 tracer simulation; only outfluxes were computed using group 2 tracers. The outflux was one way in that nitrogen species were transported out but the transport did not affect adjacent grid cells because the influxes were from group 1 tracer simulation. Using this procedure, the effects of anthropogenic NO_x emission reduction were localized. The β and γ values were computed by the ratio of TVCD and surface concentration changes to 15% change of anthropogenic NO_x emissions, respectively.

Figure 2 shows the distributions of our β and γ ratios as a function of anthropogenic NO_x emissions for July 2011 over the CONUS. Results essentially the same as Figure 2 were obtained when a perturbation of 10% was used for anthropogenic NO_x emissions. Figure S6 shows the distributions of NO_2 TVCD fraction in the boundary layer at 13:00 – 14:00 LT and 10:00 – 11:00 LT, and the fraction of soil NO_x emissions in all surface sources (soil + anthropogenic) on weekdays for July 2011, respectively. In Figure S7, we analyzed the contributions of background sources, chemical nonlinearity, and other non-emission factors (transport, NO_2 hydrolysis on aerosol chemistry, and wet and dry depositions) to the nonlinear relationships (β and γ) among anthropogenic NO_x emissions, NO_2 surface concentrations, and NO_2 TVCDs. While the model simulation is for one summer month, several key points on the surface and column concentration sensitivities to anthropogenic NO_x emissions have implications for comparing the trends of AQS and satellite TVCD data. (1) Both β and γ values are negatively correlated with anthropogenic

NO_x emissions due to chemical nonlinearity, transport, and background NO_x contributions
 (Figures 2, S6, and S7) (Gu et al., 2016; Lamsal et al., 2011). It is consistent with the distribution
 of β as a function of NO_x emissions in China (Gu et al., 2013), although the β ratios for the US
 are generally larger than for China due primarily to different emission distributions of NO_x and
 VOCs and regional circulation patterns (Zhao et al., 2009b). (2) The uncertainties of β and γ
 values increase significantly as anthropogenic NO_x emissions decrease, which means regions with
 low anthropogenic NO_x emissions are more sensitive to environmental conditions, such as NO_x
 transport from nearby regions which may even produce negative β and γ values (Figures 2 and
 S7). (3) The value of γ is generally less than β , especially for low-anthropogenic-NO_x emission
 regions, which reflects the significant contribution of free tropospheric NO₂ to NO₂ TVCD but
 not to NO₂ surface concentrations (Figures 2, S6, and S7). (4) Generally, the variations-standard
deviations of β and γ ~~values in anthropogenic NO_x emission bins~~ tend to be larger at 10:00 –
 11:00 than at 13:00 – 14:00 LT, reflecting a stronger transport effect due to weaker chemical
 losses ~~at 10:00 – 11:00 in the morning~~ (Figures 2 and S7). (5) Both β and γ values are
 significantly less than 1 at 13:00 – 14:00 LT ($\beta = 0.754$ and $\gamma = 0.84$) when anthropogenic NO_x
 emissions are $> 4 \times 10^{12}$ molecules cm⁻² s⁻¹, but they are close to 1 at 10:00 – 11:00 LT ($\beta = 0.976$
 and $\gamma = 1.032$), which reflect stronger chemistry nonlinearity at ~~13:00 – 14:00 noontime~~ than in
 the morning (Figures 2 and S7). (6) Both background sources and non-emission factors contribute
 much more to β and γ values in low-anthropogenic-NO_x emission regions than in high-
 anthropogenic-NO_x emission regions (Figure S7). (7) Chemical nonlinearity contributes much
less to β and γ values than background sources and transport effects in low-anthropogenic-NO_x
emission regions (Figure S7). ~~(87)~~ Generally, non-emission factors (mainly transport) contribute
 more to β and γ values than background sources in low-anthropogenic-NO_x emission regions
 (Figures S7c and S7d) except for the first bin where background sources contribute more to β and
 γ values than non-emission factors at 10:00 – 11:00, which is partly caused by some grid cells

with extremely low anthropogenic NO_x emissions, increasing the mean contributions of background sources in the first bin.

The largely varying β and γ values for anthropogenic NO_x emissions $< 10^{11}$ molecules cm⁻² s⁻¹ imply that the trends derived from satellite TVCD data do not directly represent anthropogenic NO_x emissions and that the variations of TVCD data may not be comparable to the corresponding surface NO₂ concentrations. We define a region “urban” if anthropogenic NO_x emissions from NEI2011 are $> 10^{11}$ molecules cm⁻² s⁻¹. All the other regions are defined as “rural”. Figure 3 shows the distributions of anthropogenic NO_x emissions and urban and rural regions defined in this study. Such defined urban regions account for 69.8% of the total anthropogenic NO_x emissions over the CONUS, the trend of which is, therefore, representative of anthropogenic emission changes. A caveat is that some “urban” regions would become “rural” if anthropogenic NO_x emissions decreased after 2011 as the EPA anthropogenic NO_x emission trend suggested (Figure S2). In a sensitivity study, we define an urban region using a stricter criterion of anthropogenic NO_x emissions $> 2 \times 10^{11}$ molecules cm⁻² s⁻¹ and the analysis results are similar to those shown in the next section.

3.2 Trend comparisons between NO₂ AQS surface concentrations and coincident satellite NO₂ tropospheric VCD over urban and rural regions

By using anthropogenic NO_x emissions of 10^{11} molecules cm⁻² s⁻¹ as the threshold value, 157 AQS sites are urban, and the rest 22 sites are rural. Their properties are summarized in Table 2. Figure 4 shows the relative annual variations of AQS NO₂ surface measurements at 13:00 – 14:00 and coincident OMI-QA4ECV NO₂ TVCD data from 2005 – 2017 in each season for urban and rural regions. The contrast between the two regions is apparent in all seasons. For comparison purposes, we scale the time series of TVCD and AQS surface NO₂ to their corresponding 2005 values, and the resulting data are therefore unitless. Over urban regions, NO₂ surface

concentrations are highly correlated with NO₂ TVCDs ($\text{TVCD} = 1.03 \times \text{AQS} + 0.11$, $R^2 = 0.98$), reflecting the comparable and stable β and γ values (Figure 2). However, over rural regions, the scaled TVCD data significantly deviate from AQS NO₂ data ($\text{TVCD} = 1.15 \times \text{AQS} + 0.09$, $R^2 = 0.87$). It is noteworthy that the discrepancies between urban and rural data are smaller in winter than in spring, summer, and autumn due to a more dominant role of transport than chemistry and lower natural NO_x emissions in winter.

We also examine the correlations of AQS NO₂ surface concentrations with coincident OMI-NASA, OMI-BEHR, SCIAMACHY, GOME-2A, and GOME-2B TVCD measurements. The results of OMI-NASA and OMI-BEHR are similar to those of OMI-QA4ECV (Figure 4). SCIAMACHY and GOME-2B TVCD observations at 9:00-11:00 LT also show large contrast between urban (SCIAMACHY: $\text{TVCD} = 0.92 \times \text{AQS} - 0.005$, $R^2 = 0.94$; GOME-2B: $\text{TVCD} = 0.54 \times \text{AQS} + 0.56$, $R^2 = 0.96$) and rural regions (SCIAMACHY: $\text{TVCD} = 0.77 \times \text{AQS} + 0.83$, $R^2 = 0.63$; GOME-2B: $\text{TVCD} = 0.46 \times \text{AQS} + 0.73$, $R^2 = 0.59$). The correlation of coincident GOME-2A NO₂ TVCD data with AQS surface concentrations is poor for rural ($\text{TVCD} = 0.65 \times \text{AQS} + 0.56$, $R^2 = 0.44$) and urban ($\text{TVCD} = 0.31 \times \text{AQS} + 0.56$, $R^2 = 0.21$) regions (Figure S8), which likely reflects the degradation of the GOME-2A instrument causing significant increase of NO₂ SCD uncertainties (Boersma et al., 2018). Therefore, we excluded GOME-2A in the analysis hereafter.

We further investigate OMI-QA4ECV NO₂ TVCD relative annual variations from 2005 - 2017 over the regions with different anthropogenic NO_x emissions in Figure 5. We find clear flattening of NO₂ TVCD variations as anthropogenic NO_x emissions decrease, which is consistent with the above analysis. Similar to Figure 4, the spread of TVCD variation is much less in winter than the other seasons. The differences between Figures 5 and 4 are due to a much larger dataset used in the former than the latter. Only coincident AQS and OMI-QA4ECV data are used in Figure 4, but all OMI-KMNI data are used in Figure 5.

3.3 Trend analysis of AQS NO₂ surface concentrations, satellite TVCDs, and updated EPA NO_x emissions

We first updated the CEMS measurement data used in the EPA NO_x emission trend datasets with the newest datasets obtained from <https://ampd.epa.gov/ampd/>. As shown in Figure S2, the updated CEMS data lead to a reduction of anthropogenic NO_x emissions during the Great Recession (2008 – 2009) and a recovery period in 2010 – 2011. The sharp drop during the Great Recession and the flattening trend right after the Great Recession are captured by OMI NO₂ and SCIAMACHY TVCD products (Figures 4, 6, and S9) and AQS NO₂ surface measurements (Figures 4, 6, and S5) and are also noted by Russell et al. (2012) and Tong et al. (2015) (Table 1).

In Figure 6, we show the comparisons among the relative variations of the updated EPA anthropogenic NO_x emissions, AQS NO₂ surface measurements at 10:00-11:00 and 13:00-14:00, and coincident satellite NO₂ TVCDs for urban regions in 4 seasons from 2003 to 2017. Also shown are the comparisons among the updated EPA anthropogenic NO_x emissions and satellite NO₂ TVCDs. There are many more data points for the latter comparison because the data selection is no longer limited to those coincident with the AQS surface data, and therefore, the uncertainty spread is much lower. The comparisons, in general, show consistent results that the updated EPA anthropogenic NO_x emissions, AQS surface measurements, and satellite TVCD data are in agreement. The agreement of decreasing trends among the datasets is just as good for the post-2011 period as the pre-2011 period. This result differs from Miyazaki et al. (2017) and Jiang et al. (2018), who suggested no significant decreasing trend for OMI TVCD data and inversed NO_x emissions after 2010. The disagreement can be explained by the results of Figure 5. Including the low anthropogenic NO_x emission regions leads to underestimates of NO_x decreases. Since the area of low anthropogenic NO_x emission regions is larger than high anthropogenic NO_x emission regions (Table 2), the arithmetic averaging will lead to a large weighting of rural observations, which do not reflect anthropogenic NO_x emission changes. Miyazaki et al. (2017)

and Jiang et al. (2018) included all regions in their analyses, but we exclude rural regions. Figure S9 shows the seasonal variations if the TVCDs over rural regions are included; the result shows a much lower decreasing rate of TVCDs over the CONUS. The much slower satellite TVCD trends for regions with low NO_x emissions was previously discussed by Zhang et al. (2018). In addition, Miyazaki et al. (2017) and Jiang et al. (2018) conducted NO_x emission inversions by using the Model for Interdisciplinary Research on Climate (MIROC)-Chem with a coarse resolution of 2.8° × 2.8°, which was insufficient to separate urban and rural regions and might distort predicted NO₂ TVCDs and inversed NO_x emissions due to nonlinear effects (Valin et al., 2011; Yu et al., 2016), which is another possible reason for their find of flattening NO_x emission trends after 2010.

We summarize the decreasing rates of NO₂ after the Great Recession in Table 3. To minimize the effect of the sharp decrease and the subsequent recovery, we chose to analyze the post-2011 period. Table 3 summarizes the results for each season, while Table 1 gives the averaged annual decreasing trends. Generally, Tables 1 and 3 confirm the continuous decreases of AQS surface observations, satellite NO₂ TVCD, and updated EPA anthropogenic NO_x emissions after 2011 as in Figure 6, but the decreasing rates are lower than the pre-2011 period. Over the AQS urban sites, the slowdown magnitudes are 9% for AQS surface observations and 20% - 40% for satellite NO₂ TVCD measurements, which may reflect in part smaller γ than β values (Table 2). Our estimated slowdown magnitudes are significantly lower than Lamsal et al. (2015) and Jiang et al. (2018) (Table 1), which might be caused by their different data processing methods, such as including AQS sites with incomplete measurement records (Silvern et al., 2019).

Over the CONUS urban regions, updated EPA anthropogenic NO_x emissions show a slowdown of 22% compared to 29% - 46% for three OMI NO₂ TVCD products. The difference is partially due to the β ratio of 2.5 ± 1.0 at 13:00 – 14:00 over the CONUS urban regions (Table 2). Satellite NO₂ TVCD measurement uncertainties also contribute to the difference. From 2013 – 2017, GOME-2B NO₂ TVCDs decrease more than OMI products, especially in spring, autumn

and winter (Tables 1 and 3). Finally, trend analyses in different regions (Figure 7 and Table S4) indicate that generally, the Midwest has the least slowdown of the decreasing rate for urban OMI NO₂ TVCD (-14% on average) after 2011 compared to the Northeast (-30%), South (-34%), and West (-28%).

The results presented in this study are qualitatively in agreement with the work by Silvern et al. (2019). The two studies were independent. Therefore, the foci of the studies are different despite reaching similar conclusions. While we focused on understanding the detailed data analysis of Jiang et al. (2018) and limited the use of model simulation results so that our results can be compared to the previous study directly, Silvern et al. (2019) relied more on multi-year model simulations. As a result, Silvern et al. (2019) can clearly identify the contributions of the NO₂ columns by natural emissions and make use of additional observations such as nitrate deposition fluxes. They also identified model biases in simulating the trends of NO₂ TVCDs by missing natural emissions in the free troposphere. Our study, on the other hand, explored the data analysis procedure through which the trend of anthropogenic emissions can be derived from satellite observations and its limitations.

4. Conclusions

Using model simulations for July 2017, we demonstrate the nonlinear relationship of NO₂ surface concentration and TVCD with anthropogenic NO_x emissions. Over low anthropogenic NO_x emission regions, the ratios of anthropogenic NO_x emission changes to the changes of surface concentrations (γ) and TVCDs (β) have very large variations and $\beta > \gamma \gg 1$. Therefore, for the same emission changes, surface concentration and TVCD changes are much smaller and variable than urban regions, making it difficult to use the observations to directly infer anthropogenic NO_x emission trends. We find that defining urban regions where anthropogenic NO_x emissions are $> 10^{11}$ molecules cm⁻² s⁻¹ and using surface and TVCD

observations over these regions can infer the trends that can be compared with the EPA emission trend estimates.

We evaluate the anthropogenic NO_x emission variations from 2003 – 2017 over the CONUS by using satellite NO₂ TVCD products from GOME-2B, SCIAMACHY, OMI-QA4ECV, OMI-NASA, and OMI-BEHR, over the urban regions of CONUS. We find broad agreements among the decreases of AQS NO₂ surface observations, satellite NO₂ TVCD products, and the EPA anthropogenic NO_x emissions with the CEMS dataset updated. After 2011, they all show a slowdown of the decreasing rates. Over the AQS urban sites, NO₂ surface concentrations have a slowdown of 9% and OMI products show a slowdown of 20% - 40%. Over the CONUS urban regions, OMI TVCD products indicate a slowdown of 29% - 46%, and the updated EPA anthropogenic NO_x emissions have a slowdown of 22%. The different slowdown magnitudes between OMI TVCD products and the other two datasets may be caused by the nonlinear response of TVCD to anthropogenic emissions and the uncertainties of satellite measurements (e.g., GOME-2B TVCD data show a larger decreasing trend than OMI products from 2013 – 2017).

We did not find observation evidence supporting the notion that anthropogenic NO_x emissions have not been decreasing after the Great Recession. In future studies, we recommend that the nonlinear relationships of NO_x emissions with NO₂ TVCD and surface concentration be carefully evaluated when applying satellite and surface measurements to infer the changes of anthropogenic NO_x emissions.

Data availability

The EPA AQS hourly surface NO₂ measurements are downloaded from https://aq5.epa.gov/aqsweb/airdata/download_files.html#Raw. QA4ECV 1.1 NO₂ VCD products

(OMI-QA4ECV, GOME-2A, and SCIAMACHY) are from <http://temis.nl/qa4ecv/no2col/data/>.
GOME-2B NO₂ VCD products are from
<http://www.temis.nl/airpollution/no2col/no2colgome2b.php>. OMI-BEHR and OMI-NASA
archives are from <http://behr.cchem.berkeley.edu/DownloadBEHRData.aspx>. REAM simulation
results for this study are available upon request.

Author contribution

JL and YW designed the study. JL conducted model simulations and data analyses with
discussions with YW. JL and YW wrote the manuscript.

Competing interests

The authors declare that they have no conflict of interest.

Acknowledgments

This work was supported by the NASA ACMAP Program. We thank Ruixiong Zhang for
discussions with J. Li. Thank Benjamin Wells, Alison Eyth, Lee Tooty from EPA, the EPA
MOVES team, Betty Carter from COORDINATING RESEARCH COUNCIL, INC., Brian
McDonald from NOAA, and Zhe Jiang from University of Science and Technology of China for
helping us an understanding of the NEI MOVES mobile source emissions.

References

- Alkuwari, F. A., Guillas, S., and Wang, Y.: Statistical downscaling of an air quality model using
Fitted Empirical Orthogonal Functions, *Atmos. Environ.*, 81, 1-10,
<https://doi.org/10.1016/j.atmosenv.2013.08.031>, 2013.
- Beaver, M., Long, R., and Kronmiller, K.: Characterization and Development of Measurement
Methods for Ambient Nitrogen Dioxide (NO₂), National Air Quality Conference - Ambient Air
Monitoring 2012, Denver, CO, US, 2012.

438 Beaver, M., Kronmiller, K., Duvall, R., Kaushik, S., Morphy, T., King, P., and Long, R.: Direct
 439 and Indirect Methods for the Measurement of Ambient Nitrogen Dioxide, AWMA Measurement
 440 Technologies meeting, Sacramento, CA, US, 2013.

441 Beirle, S., Platt, U., Wenig, M., and Wagner, T.: Weekly cycle of NO₂ by GOME measurements:
 442 A signature of anthropogenic sources, *Atmos. Chem. Phys.*, 3, 2225-2232,
 443 <https://doi.org/10.5194/acp-3-2225-2003>, 2003.

444 Bishop, G. A., and Stedman, D. H.: Reactive nitrogen species emission trends in three light-
 445 /medium-duty United States fleets, *Environ. Sci. Technol.*, 49, 11234-11240,
 446 <https://doi.org/10.1021/acs.est.5b02392>, 2015.

447 Boersma, K. F., Eskes, H. J., Richter, A., De Smedt, I., Lorente, A., Beirle, S., van Geffen, J. H.,
 448 Zara, M., Peters, E., and Roozendaal, M. V.: Improving algorithms and uncertainty estimates for
 449 satellite NO₂ retrievals: results from the quality assurance for the essential climate variables
 450 (QA4ECV) project, *Atmos. Meas. Tech.*, 11, 6651-6678, [https://doi.org/10.5194/amt-11-6651-](https://doi.org/10.5194/amt-11-6651-2018)
 451 2018, 2018.

452 Cheng, Y., Wang, Y., Zhang, Y., Chen, G., Crawford, J. H., Kleb, M. M., Diskin, G. S., and
 453 Weinheimer, A. J.: Large biogenic contribution to boundary layer O₃-CO regression slope in
 454 summer, *Geophys. Res. Lett.*, 44, 7061-7068, <https://doi.org/10.1002/2017GL074405>, 2017.

455 Cheng, Y., Wang, Y., Zhang, Y., Crawford, J. H., Diskin, G. S., Weinheimer, A. J., and Fried, A.:
 456 Estimator of surface ozone using formaldehyde and carbon monoxide concentrations over the
 457 eastern United States in summer, *J. Geophys. Res.-Atmos.*, 123, 7642-7655,
 458 <https://doi.org/10.1029/2018JD028452>, 2018.

459 Choi, Y., Wang, Y., Zeng, T., Martin, R. V., Kurosu, T. P., and Chance, K.: Evidence of lightning
 460 NO_x and convective transport of pollutants in satellite observations over North America,
 461 *Geophys. Res. Lett.*, 32, <https://doi.org/10.1029/2004GL021436>, 2005.

462 Choi, Y., Wang, Y., Yang, Q., Cunnold, D., Zeng, T., Shim, C., Luo, M., Eldering, A., Bucsela,
 463 E., and Gleason, J.: Spring to summer northward migration of high O₃ over the western North
 464 Atlantic, *Geophys. Res. Lett.*, 35, <https://doi.org/10.1029/2007GL032276>, 2008a.

465 Choi, Y., Wang, Y., Zeng, T., Cunnold, D., Yang, E. S., Martin, R., Chance, K., Thouret, V., and
 466 Edgerton, E.: Springtime transitions of NO₂, CO, and O₃ over North America: Model evaluation
 467 and analysis, *J. Geophys. Res.-Atmos.*, 113, <https://doi.org/10.1029/2007JD009632>, 2008b.

468 Choi, Y., Kim, H., Tong, D., and Lee, P.: Summertime weekly cycles of observed and modeled
 469 NO_x and O₃ concentrations as a function of satellite-derived ozone production sensitivity and land
 470 use types over the Continental United States, *Atmos. Chem. Phys.*, 12, 6291-6307,
 471 <https://doi.org/10.5194/acp-12-6291-2012>, 2012.

472 Crouse, D. L., Peters, P. A., Hystad, P., Brook, J. R., van Donkelaar, A., Martin, R. V.,
 473 Villeneuve, P. J., Jerrett, M., Goldberg, M. S., and Pope III, C. A.: Ambient PM_{2.5}, O₃, and NO₂
 474 exposures and associations with mortality over 16 years of follow-up in the Canadian Census
 475 Health and Environment Cohort (CanCHEC), *Environ. Health Perspect.*, 123, 1180,
 476 <https://doi.org/10.1289/ehp.1409276>, 2015.

477 De Gouw, J. A., Parrish, D. D., Frost, G. J., and Trainer, M.: Reduced emissions of CO₂, NO_x,
 478 and SO₂ from US power plants owing to switch from coal to natural gas with combined cycle
 479 technology, *Earth's Future*, 2, 75-82, <https://doi.org/10.1002/2013EF000196>, 2014.

480 Drosoglou, T., Bais, A. F., Zyrichidou, I., Kouremeti, N., Poupkou, A., Liora, N., Giannaros, C.,
 481 Koukouli, M. E., Balis, D., and Melas, D.: Comparisons of ground-based tropospheric NO₂
 482 MAX-DOAS measurements to satellite observations with the aid of an air quality model over the
 483 Thessaloniki area, Greece, *Atmos. Chem. Phys.*, 17, 5829-5849, [https://doi.org/10.5194/acp-17-](https://doi.org/10.5194/acp-17-5829-2017)
 484 5829-2017, 2017.

485 Drosoglou, T., Koukouli, M. E., Kouremeti, N., Bais, A. F., Zyrichidou, I., Balis, D., Xu, J., and
 486 Li, A.: MAX-DOAS NO₂ observations over Guangzhou, China; ground-based and satellite
 487 comparisons, *Atmos. Meas. Tech.*, 11, 2239-2255, <https://doi.org/10.5194/amt-11-2239-2018>,
 488 2018.

489 EPA: PROFILE OF VERSION 1 OF THE 2014 NATIONAL EMISSIONS INVENTORY, U.S.
 490 Environmental Protection Agency, 2017.

491 Air Pollutant Emissions Trends Data: [https://www.epa.gov/air-emissions-inventories/air-](https://www.epa.gov/air-emissions-inventories/air-pollutant-emissions-trends-data)
 492 [pollutant-emissions-trends-data](https://www.epa.gov/air-emissions-inventories/air-pollutant-emissions-trends-data), 2018.

493 Fisher, J. A., Jacob, D. J., Travis, K. R., Kim, P. S., Marais, E. A., Chan Miller, C., Yu, K., Zhu,
 494 L., Yantosca, R. M., and Sulprizio, M. P.: Organic nitrate chemistry and its implications for
 495 nitrogen budgets in an isoprene-and monoterpene-rich atmosphere: constraints from aircraft
 496 (SEAC⁴RS) and ground-based (SOAS) observations in the Southeast US, *Atmos. Chem. Phys.*,
 497 16, 5969-5991, <https://doi.org/10.5194/acp-16-5969-2016>, 2016.

498 Georgoulas, A. K., van der A, R. J., Stammes, P., Boersma, K. F., and Eskes, H. J.: Trends and
 499 trend reversal detection in 2 decades of tropospheric NO₂ satellite observations, *Atmos. Chem.*
 500 *Phys.*, 19, 6269-6294, <https://doi.org/10.5194/acp-19-6269-2019>, 2019.

501 Greenberg, N., Carel, R. S., Derazne, E., Bibi, H., Shpriz, M., Tzur, D., and Portnov, B. A.:
 502 Different effects of long-term exposures to SO₂ and NO₂ air pollutants on asthma severity in
 503 young adults, *J. Toxicol. Environ. Health, A*, 79, 342-351,
 504 <https://doi.org/10.1080/15287394.2016.1153548>, 2016.

505 Greenberg, N., Carel, R. S., Derazne, E., Tiktinsky, A., Tzur, D., and Portnov, B. A.: Modeling
 506 long-term effects attributed to nitrogen dioxide (NO₂) and sulfur dioxide (SO₂) exposure on
 507 asthma morbidity in a nationwide cohort in Israel, *J. Toxicol. Environ. Health, A*, 80, 326-337,
 508 <https://doi.org/10.1080/15287394.2017.1313800>, 2017.

509 Gu, D., Wang, Y., Smeltzer, C., and Liu, Z.: Reduction in NO_x emission trends over China:
 510 Regional and seasonal variations, *Environ. Sci. Technol.*, 47, 12912-12919,
 511 <https://doi.org/10.1021/es401727e>, 2013.

512 Gu, D., Wang, Y., Smeltzer, C., and Boersma, K. F.: Anthropogenic emissions of NO_x over
 513 China: Reconciling the difference of inverse modeling results using GOME-2 and OMI
 514 measurements, *J. Geophys. Res.-Atmos.*, 119, 7732-7740,
 515 <https://doi.org/10.1002/2014JD021644>, 2014.

516 Gu, D., Wang, Y., Yin, R., Zhang, Y., and Smeltzer, C.: Inverse modelling of NO_x emissions over
 517 eastern China: uncertainties due to chemical non-linearity, *Atmos. Meas. Tech.*, 9, 5193-5201,
 518 <https://doi.org/10.5194/amt-9-5193-2016>, 2016.

519 Guenther, A. B., Jiang, X., Heald, C. L., Sakulyanontvittaya, T., Duhl, T., Emmons, L. K., and
 520 Wang, X.: The Model of Emissions of Gases and Aerosols from Nature version 2.1
 521 (MEGAN2.1): an extended and updated framework for modeling biogenic emissions, *Geosci.*
 522 *Model Dev.*, 5, 1471-1492, <https://doi.org/10.5194/gmd-5-1471-2012>, 2012.

523 Hassler, B., McDonald, B. C., Frost, G. J., Borbon, A., Carslaw, D. C., Civerolo, K., Granier, C.,
 524 Monks, P. S., Monks, S., and Parrish, D. D.: Analysis of long-term observations of NO_x and CO
 525 in megacities and application to constraining emissions inventories, *Geophys. Res. Lett.*, 43,
 526 9920-9930, <https://doi.org/10.1002/2016GL069894>, 2016.

527 Heinrich, J., Thiering, E., Rzehak, P., Krämer, U., Hochadel, M., Rauchfuss, K. M., Gehring, U.,
 528 and Wichmann, H.-E.: Long-term exposure to NO₂ and PM₁₀ and all-cause and cause-specific
 529 mortality in a prospective cohort of women, *Occup. Environ. Med.*, 70, 179-186,
 530 <https://doi.org/10.1136/oemed-2012-100876>, 2013.

531 Jiang, Z., McDonald, B. C., Worden, H., Worden, J. R., Miyazaki, K., Qu, Z., Henze, D. K.,
 532 Jones, D. B. A., Arellano, A. F., and Fischer, E. V.: Unexpected slowdown of US pollutant
 533 emission reduction in the past decade, *Proc. Natl. Acad. Sci. U.S.A.*, 201801191,
 534 <https://doi.org/10.1073/pnas.1801191115>, 2018.

535 Kampa, M., and Castanas, E.: Human health effects of air pollution, *Environ. Pollut.*, 151, 362-
 536 367, <https://doi.org/10.1016/j.envpol.2007.06.012>, 2008.

537 Kebabian, P. L., Herndon, S. C., and Freedman, A.: Detection of nitrogen dioxide by cavity
 538 attenuated phase shift spectroscopy, *Anal. Chem.*, 77, 724-728,
 539 <https://doi.org/10.1021/ac048715y>, 2005.

540 Koo, J.-H., Wang, Y., Kurosu, T. P., Chance, K., Rozanov, A., Richter, A., Oltmans, S. J.,
 541 Thompson, A. M., Hair, J. W., and Fenn, M. A.: Characteristics of tropospheric ozone depletion
 542 events in the Arctic spring: analysis of the ARCTAS, ARCPAC, and ARCIONS measurements
 543 and satellite BrO observations, *Atmos. Chem. Phys.*, 12, 9909-9922, <https://doi.org/10.5194/acp-12-9909-2012>, 2012.

545 Krotkov, N. A., Lamsal, L. N., Celarier, E. A., Swartz, W. H., Marchenko, S. V., Bucsela, E. J.,
 546 Chan, K. L., Wenig, M., and Zara, M.: The version 3 OMI NO₂ standard product, *Atmos. Meas.*
 547 *Tech.*, 10, 3133-3149, <https://doi.org/10.5194/amt-10-3133-2017>, 2017.

548 Lamsal, L. N., Martin, R. V., Padmanabhan, A., Van Donkelaar, A., Zhang, Q., Sioris, C. E.,
 549 Chance, K., Kurosu, T. P., and Newchurch, M. J.: Application of satellite observations for timely
 550 updates to global anthropogenic NO_x emission inventories, *Geophys. Res. Lett.*, 38,
 551 <https://doi.org/10.1029/2010GL046476>, 2011.

552 Lamsal, L. N., Duncan, B. N., Yoshida, Y., Krotkov, N. A., Pickering, K. E., Streets, D. G., and
 553 Lu, Z.: US NO₂ trends (2005–2013): EPA Air Quality System (AQS) data versus improved
 554 observations from the Ozone Monitoring Instrument (OMI), *Atmos. Environ.*, 110, 130-143,
 555 <https://doi.org/10.1016/j.atmosenv.2015.03.055>, 2015.

Laughner, J. L., Zhu, Q., and Cohen, R. C.: The Berkeley High Resolution Tropospheric NO₂ product, Earth System Science Data, 10, 2069-2095, <https://doi.org/10.5194/essd-10-2069-2018>, 2018.

Li, J., Mao, J., Fiore, A. M., Cohen, R. C., Crounse, J. D., Teng, A. P., Wennberg, P. O., Lee, B. H., Lopez-Hilfiker, F. D., and Thornton, J. A.: Decadal changes in summertime reactive oxidized nitrogen and surface ozone over the Southeast United States, Atmos. Chem. Phys., 18, 2341-2361, <https://doi.org/10.5194/acp-18-2341-2018>, 2018.

Li, J., Wang, Y., and Qu, H.: Dependence of summertime surface ozone on NO_x and VOC emissions over the United States: Peak time and value, Geophys. Res. Lett., 46, 3540-3550, <https://doi.org/10.1029/2018GL081823>, 2019.

Liu, Z., Wang, Y., Vrekoussis, M., Richter, A., Wittrock, F., Burrows, J. P., Shao, M., Chang, C. C., Liu, S. C., and Wang, H.: Exploring the missing source of glyoxal (CHOCHO) over China, Geophys. Res. Lett., 39, <https://doi.org/10.1029/2012GL051645>, 2012.

Liu, Z., Wang, Y., Costabile, F., Amoroso, A., Zhao, C., Huey, L. G., Stickel, R., Liao, J., and Zhu, T.: Evidence of aerosols as a media for rapid daytime HONO production over China, Environ. Sci. Technol., 48, 14386-14391, <https://doi.org/10.1021/es504163z>, 2014.

Luo, C., Wang, Y., and Koshak, W. J.: Development of a self-consistent lightning NO_x simulation in large-scale 3-D models, J. Geophys. Res.-Atmos., 122, 3141-3154, <https://doi.org/10.1002/2016JD026225>, 2017.

McDonald, B., McKeen, S., Cui, Y. Y., Ahmadov, R., Kim, S.-W., Frost, G. J., Pollack, I., Peischl, J., Ryerson, T. B., and Holloway, J.: Modeling Ozone in the Eastern US using a Fuel-Based Mobile Source Emissions Inventory, Environ. Sci. Technol., <https://doi.org/10.1021/acs.est.8b00778>, 2018.

Miyazaki, K., Eskes, H., Sudo, K., Boersma, K. F., Bowman, K., and Kanaya, Y.: Decadal changes in global surface NO_x emissions from multi-constituent satellite data assimilation, Atmos. Chem. Phys., 17, 807-837, <https://doi.org/10.5194/acp-17-807-2017>, 2017.

Myhre, G., Shindell, D., Bréon, F.-M., Collins, W., Fuglestad, J., Huang, J., Koch, D., Lamarque, J.-F., Lee, D., Mendoza, B., Nakajima, T., Robock, A., Stephens, G., Takemura, T., and Zhang, H.: Anthropogenic and natural radiative forcing, in: Climate change 2013: The Physical Science Basis. Contribution of Working Group I to the Fifth Assessment Report of the Intergovernmental Panel on Climate Change, Cambridge University Press, Cambridge, United Kingdom and New York, NY, USA, 659-740, 2013.

Pandey, J. S., Kumar, R., and Devotta, S.: Health risks of NO₂, SPM and SO₂ in Delhi (India), Atmos. Environ., 39, 6868-6874, <https://doi.org/10.1016/j.atmosenv.2005.08.004>, 2005.

Price, C., and Rind, D.: A simple lightning parameterization for calculating global lightning distributions, J. Geophys. Res.-Atmos., 97, 9919-9933, <https://doi.org/10.1029/92JD00719>, 1992.

Russell, A. R., Valin, L. C., and Cohen, R. C.: Trends in OMI NO₂ observations over the United States: effects of emission control technology and the economic recession, Atmos. Chem. Phys., 12, 12197-12209, <https://doi.org/10.5194/acp-12-12197-2012>, 2012.

Seinfeld, J. H., and Pandis, S. N.: Atmospheric chemistry and physics: from air pollution to climate change, John Wiley & Sons, Inc, Hoboken, New Jersey, 2016.

Silvern, R. F., Jacob, D. J., Mickley, L. J., Sulprizio, M. P., Travis, K. R., Marais, E. A., Cohen, R. C., Laughner, J. L., Choi, S., Joiner, J., and Lamsal, L. N.: Using satellite observations of tropospheric NO₂ columns to infer long-term trends in US NO_x emissions: the importance of accounting for the free tropospheric NO₂ background, *Atmos. Chem. Phys.*, 19, 8863-8878, <https://doi.org/10.5194/acp-19-8863-2019>, 2019.

Singh, A., and Agrawal, M.: Acid rain and its ecological consequences, *J. Environ. Biol.*, 29, 15, 2007.

Tong, D., Lamsal, L., Pan, L., Ding, C., Kim, H., Lee, P., Chai, T., Pickering, K. E., and Stajner, I.: Long-term NO_x trends over large cities in the United States during the great recession: Comparison of satellite retrievals, ground observations, and emission inventories, *Atmos. Environ.*, 107, 70-84, <https://doi.org/10.1016/j.atmosenv.2015.01.035>, 2015.

Valin, L. C., Russell, A. R., Hudman, R. C., and Cohen, R. C.: Effects of model resolution on the interpretation of satellite NO₂ observations, *Atmos. Chem. Phys.*, 11, 11647-11655, <https://doi.org/10.5194/acp-11-11647-2011>, 2011.

Wang, Y., Choi, Y., Zeng, T., Davis, D., Buhr, M., Huey, L. G., and Neff, W.: Assessing the photochemical impact of snow NO_x emissions over Antarctica during ANTICI 2003, *Atmos. Environ.*, 41, 3944-3958, <https://doi.org/10.1016/j.atmosenv.2007.01.056>, 2007.

Wang, Y., Beirle, S., Lampel, J., Koukouli, M., De Smedt, I., Theys, N., Ang, L., Wu, D., Xie, P., and Liu, C.: Validation of OMI, GOME-2A and GOME-2B tropospheric NO₂, SO₂ and HCHO products using MAX-DOAS observations from 2011 to 2014 in Wuxi, China: investigation of the effects of priori profiles and aerosols on the satellite products, *Atmos. Chem. Phys.*, 17, 5007, <https://doi.org/10.5194/acp-17-5007-2017>, 2017.

Weinmayr, G., Romeo, E., De Sario, M., Weiland, S. K., and Forastiere, F.: Short-term effects of PM₁₀ and NO₂ on respiratory health among children with asthma or asthma-like symptoms: a systematic review and meta-analysis, *Environ. Health Perspect.*, 118, 449-457, <https://doi.org/10.1289/ehp.0900844>, 2009.

Xing, J., Pleim, J., Mathur, R., Pouliot, G., Hogrefe, C., Gan, C. M., and Wei, C.: Historical gaseous and primary aerosol emissions in the United States from 1990 to 2010, *Atmos. Chem. Phys.*, 13, 7531-7549, <https://doi.org/10.5194/acp-13-7531-2013>, 2013.

Yang, Q., Wang, Y., Zhao, C., Liu, Z., Gustafson Jr, W. I., and Shao, M.: NO_x emission reduction and its effects on ozone during the 2008 Olympic Games, *Environ. Sci. Technol.*, 45, 6404-6410, <https://doi.org/10.1021/es200675v>, 2011.

Yienger, J. J., and Levy, H.: Empirical model of global soil-biogenic NO_x emissions, *J. Geophys. Res.-Atmos.*, 100, 11447-11464, <https://doi.org/10.1029/95JD00370>, 1995.

Yu, K., Jacob, D. J., Fisher, J. A., Kim, P. S., Marais, E. A., Miller, C. C., Travis, K. R., Zhu, L., Yantosca, R. M., and Sulprizio, M. P.: Sensitivity to grid resolution in the ability of a chemical

633 transport model to simulate observed oxidant chemistry under high-isoprene conditions, *Atmos.*
634 *Chem. Phys.*, 16, 4369-4378, <https://doi.org/10.5194/acp-16-4369-2016>, 2016.

635 Zara, M., Boersma, K. F., De Smedt, I., Richter, A., Peters, E., Van Geffen, J. H. G. M., Beirle,
636 S., Wagner, T., Van Roozendael, M., and Marchenko, S.: Improved slant column density retrieval
637 of nitrogen dioxide and formaldehyde for OMI and GOME-2A from QA4ECV: intercomparison,
638 uncertainty characterization, and trends, *Meas. Tech. Discuss.*, 1-47, [https://doi.org/10.5194/amt-](https://doi.org/10.5194/amt-11-4033-2018)
639 11-4033-2018, 2018.

640 Zhang, R., Wang, Y., He, Q., Chen, L., Zhang, Y., Qu, H., Smeltzer, C., Li, J., Alvarado, L., and
641 Vrekoussis, M.: Enhanced trans-Himalaya pollution transport to the Tibetan Plateau by cut-off
642 low systems, *Atmos. Chem. Phys.*, 17, 3083-3095, <https://doi.org/10.5194/acp-17-3083-2017>,
643 2017.

644 Zhang, R., Wang, Y., Smeltzer, C., Qu, H., Koshak, W., and Boersma, K. F.: Comparing OMI-
645 based and EPA AQS in situ NO₂ trends: towards understanding surface NO_x emission changes,
646 *Atmos. Meas. Tech.*, 11, 3955-3967, <https://doi.org/10.5194/amt-11-3955-2018>, 2018.

647 Zhang, Y., and Wang, Y.: Climate-driven ground-level ozone extreme in the fall over the
648 Southeast United States, *Proc. Natl. Acad. Sci. U.S.A.*, 113, 10025-10030,
649 <https://doi.org/10.1073/pnas.1602563113>, 2016.

650 Zhao, C., and Wang, Y.: Assimilated inversion of NO_x emissions over east Asia using OMI NO₂
651 column measurements, *Geophys. Res. Lett.*, 36, <https://doi.org/10.1029/2008GL037123>, 2009.

652 Zhao, C., Wang, Y., Choi, Y., and Zeng, T.: Summertime impact of convective transport and
653 lightning NO_x production over North America: modeling dependence on meteorological
654 simulations, *Atmos. Chem. Phys.*, 9, 4315-4327, <https://doi.org/10.5194/acp-9-4315-2009>, 2009a.

655 Zhao, C., Wang, Y., and Zeng, T.: East China plains: A “basin” of ozone pollution, *Environ. Sci.*
656 *Technol.*, 43, 1911-1915, <https://doi.org/10.1021/es8027764>, 2009b.

657 Zhao, C., Wang, Y., Yang, Q., Fu, R., Cunnold, D., and Choi, Y.: Impact of East Asian summer
658 monsoon on the air quality over China: View from space, *J. Geophys. Res.-Atmos.*, 115,
659 <https://doi.org/10.1029/2009JD012745>, 2010.

660

Table 1. Summary of trends of satellite NO₂ TVCD products, NO₂ surface measurements, and EPA anthropogenic NO_x emissions during from different studies

| Studies | Datasets | Period 1 ¹ | | Period 2 | | Period 3 | | Slowdown ratio ³ |
|--|--|-----------------------|--|-------------|---------------------------|-------------|------------------------------|-----------------------------|
| | | Time | Trend (yr ⁻¹) ² | Time | Trend (yr ⁻¹) | Time | Trend (yr ⁻¹) | |
| This study for CONUS “urban” sites ⁴ | GOME-2B ⁵ (36 × 36 km ²) | | | | | 2013 - 2017 | -8.2 ± 3.0% | |
| | SCIAMACHY (36 × 36 km ²) | 2003 – 2011 | -6.3 ± 1.1% | | | | | |
| | OMI-NASA (36 × 36 km ²) | 2005 – 2011 | -8.6 ± 1.2% | | | 2011 – 2016 | -6.1 ± 3.6% | -29%² |
| | OMI-BEHR (36 × 36 km ²) | 2005 – 2011 | -8.2 ± 1.3% | | | 2011 – 2016 | -4.4 ± 1.6% | -46% |
| | OMI-QA4ECV (36 × 36 km ²) | 2005 – 2011 | -7.7 ± 1.4% | | | 2011 - 2017 | -4.2 ± 0.5% | -46% |
| | Updated EPA NO _x emissions ⁶ | 2003 – 2011 | -6.5 ± 0.8% | | | 2011 - 2017 | -5.1 ± 0.3% | -22% |
| This study for AQS “urban” sites | GOME-2B (36 × 36 km ²) | | | | | 2013 - 2017 | -10.2 ± 2.9% | |
| | SCIAMACHY (36 × 36 km ²) | 2003 - 2011 | -7.6 ± 1.1% | | | | | |
| | OMI-NASA (36 × 36 km ²) | 2005 - 2011 | -9.0 ± 0.8% | | | 2011 – 2016 | -7.2 ± 3.8% | -20% |
| | OMI-BEHR (36 × 36 km ²) | 2005 - 2011 | -8.9 ± 0.3% | | | 2011 – 2016 | -6.2 ± 2.6% | -30% |
| | OMI-QA4ECV (36 × 36 km ²) | 2005 - 2011 | -9.0 ± 0.8% | | | 2011 - 2017 | -5.4 ± 0.9% | -40% |
| | NO ₂ surface VMR ⁷ | 2003 - 2011 | -6.5 ± 1.2% | | | 2011 - 2017 | -5.9 ± 0.8% | -9% |
| (Russell et al., 2012) ⁸ | BEHR v2.1 NO ₂ TVCD (0.05°×0.05°) | 2005 - 2007 | -6 ± 5% (-6.2%) ⁹ | 2007 - 2009 | -8 ± 5% (-8.4%) | 2009 - 2011 | -3 ± 4% (-3.0%) | -52% |
| | Updated EPA NO _x emissions | | -6.0% | | -10.0% | | -2.4% | -60% |
| (Tong et al., 2015) ¹⁰ | NASA v2.1 NO ₂ TVCD (pixels < 50 × 24 km ²) | | -7.3% (-7.6%) | | -9.2% (-11.4%) | | -2.8% (-4.4%) | -42% |
| | BEHR v2.1 NO ₂ TVCD (pixels < 50 × 24 km ²) | 2005 - 2007 | -8.9% (-9.3%) | 2008 - 2009 | -9.1% (-11.8%) | 2010 - 2012 | -3.6% (-6.0%) | -35% |
| | NO ₂ surface VMR | | -6.0% (-6.2%) | | -10.8% (-13.2%) | | -3.4% (-5.4%) | -13% |
| | Updated EPA NO _x emissions | | -6.0% | | -10.0% | | -3.4% | -43% |
| (Lamsal et al., 2015) ¹¹ | NASA v2.1 NO ₂ TVCD (0.1°×0.1°) | | -4.8 ± 1.9% (-5.1%) | | | | -1.2 ± 1.2% (-1.2%) | -76% |
| | NO ₂ surface VMR | 2005 - 2008 | -3.7 ± 1.5% (-3.8%) | | | 2010 - 2013 | -2.1 ± 1.4% (-2.1%) | -45% |
| | Updated EPA NO _x emissions | | -6.4% | | | | -4.0% | -38% |
| (Jiang et al., 2018) ¹¹ | NASA v3 NO ₂ TVCD (0.5°×0.667°) | | -10.2 ± 1.8% (-9.8%) | | | | -3.2 ± 1.6% (-3.2%) | -67% |
| | QA4ECV v2 NO ₂ TVCD (0.5°×0.667°) | | -9.6 ± 1.7% (-9.3%) | | | | -2.6 ± 1.8% (-2.6%) | -72% |
| | BEHR v2.1 NO ₂ TVCD (0.5°×0.667°) | 2005 - 2009 | -8.5 ± 1.8% (-8.2%) | | | 2011-2015 | -2.1 ± 1.6% (-2.1%) | -74% |
| | NO ₂ surface VMR | | -6.6 ± 1.4% (-6.4%) | | | | -2.6 ± 1.5% (-2.6%) | -59% |
| | Updated EPA NO _x emissions | | -7.8% | | | | -5.0% | -36% |

662

¹ Since different studies used different time division methods, we list the period of each study in the table.

663

² Trends are based on an exponential model ($E(y) = E_0 \times r^{y-y_0}$: “y” denotes year and “y₀” denotes the initial year; “E(y)” denotes the value at year “y” and “E₀” denotes the value at the initial year; r-1 is the relative trend).

664

³ Slowdown ratios = Trend in “period 3” / Trend in “period 1” – 1.

665

⁴ Trends in our study are calculated based on the national seasonal trends shown in Table 3.

666

⁵ The information on satellite products used in this study is summarized in Table S2.

667

⁶ We updated EPA anthropogenic NO_x emissions with the newest Continuous Emission Monitoring Systems (CEMS) datasets. Figure S2 shows the comparison between our updated and original EPA anthropogenic NO_x emissions (EPA, 2018).

668

⁷ Denote the averaged trends of 13:00 and 10:00 LT based on the values in Table 3.

669 ⁸ The study used NO₂ TVCD from urban and power plant grid cells across the U.S.

670 ⁹ Since previous studies used linear models to calculate trends and the results are sensitive to their calculation methods and the selection of initial years, we recalculate the trends based on the above exponential model, which makes all the results

671 consistent. Our results are those bold numbers inside the parentheses, while the numbers in normal fonts are from the original publications.

672 ¹⁰ The study uses NO₂ TVCD and surface concentrations from Los Angeles, Dallas, Houston, Atlanta, Philadelphia, Washington, D.C., New York, and Boston.

673 ¹¹ The two studies used the EPA Air Quality System (AQS) NO₂ surface measurements and coincident satellite NO₂ TVCD data over the U.S.

674 **Table 2.** Properties of urban and rural regions in July 2011

| type | Surface area fraction ¹ | Anthropogenic NO _x emissions ($\times 10^{10}$ molecules cm ⁻² s ⁻¹) | β at 13:00 – 14:00 LT | γ at 13:00 – 14:00 LT | β at 10:00 – 11:00 LT | γ at 10:00 – 11:00 LT |
|--------------------------|---------------------------------------|--|-----------------------------|------------------------------|-----------------------------|------------------------------|
| Urban/CONUS ² | 17.3% | 29.9 | 2.5 ± 1.0 | 1.5 ± 0.4 | 2.6 ± 1.9 | 1.6 ± 1.2 |
| Rural/CONUS | 82.7% | 2.7 | 16.9 ± 16.4 | 8.5 ± 11.7 | 12.2 ± 14.0 | 6.4 ± 11.6 |
| Urban/AQS | 87.7% | 71.0 | 1.6 ± 0.8 | 1.2 ± 0.4 | 1.7 ± 1.1 | 1.3 ± 0.6 |
| Rural/AQS | 12.3% | 5.7 | 8.7 ± 9.9 | 5.2 ± 8.8 | 5.4 ± 15.1 | 3.8 ± 11.7 |

675 ¹ “Fraction” denotes the percentages of “urban” or “rural” data points for the whole CONUS or all AQS sites.

676 ² “Urban-CONUS” denote CONUS “urban” grid cells; “Urban-AQS” denote AQS “urban” site grid cells.

677
678

679

680

Table 3. Summary of national trends of updated EPA anthropogenic NO_x emissions, AQS NO₂ surface concentrations at 13:00 – 14:00 and 10:00 – 11:00 LT, and satellite NO₂ TVCD products for 4 seasons during different periods¹

| | | Spring | | Summer | | Autumn | | Winter | |
|--|-------------|--------------|--------------|--------------|-------------|---------------|--------------|---------------|---------------|
| | | AQS site | CONUS | AQS site | CONUS | AQS site | CONUS | AQS site | CONUS |
| AQS NO ₂ VMR at 13:00 -14:00 | 2003 – 2011 | -7.3 ± 1.4% | | -7.4 ± 0.9% | | -6.7 ± 1.8% | | -5.2 ± 0.8% | |
| | 2011 – 2017 | -5.3 ± 1.6% | | -6.4 ± 1.2% | | -7.3 ± 2.5% | | -6.0 ± 2.8% | |
| AQS NO ₂ VMR at 10:00 – 11:00 | 2003 – 2011 | -7.1 ± 1.6% | | -7.6 ± 1.5% | | -6.2 ± 2.2% | | -4.4 ± 1.6% | |
| | 2011 – 2017 | -4.4 ± 1.4% | | -6.1 ± 1.8% | | -6.3 ± 2.5% | | -5.2 ± 2.4% | |
| SCIAMACHY | 2003 – 2011 | -8.8 ± 3.4% | -6.9 ± 1.1% | -8.2 ± 1.6% | -5.2 ± 1.2% | -6.8 ± 2.4% | -5.6 ± 2.1% | -6.4 ± 7.4% | -7.5 ± 5.5% |
| | 2011 – 2017 | | | | | | | | |
| GOME2B | 2003 – 2011 | | | | | | | | |
| | 2013 – 2017 | -10.2 ± 7.8% | -8.3 ± 16.9% | -6.4 ± 14.0% | -5.3 ± 4.0% | -10.5 ± 41.6% | -6.9 ± 13.2% | -13.6 ± 15.1% | -12.3 ± 78.9% |
| OMI-QA4ECV | 2005 – 2011 | -9.3 ± 5.6% | -8.3 ± 4.6% | -8.3 ± 2.4% | -5.9 ± 5.2% | -10.0 ± 4.2% | -7.4 ± 2.4% | -8.3 ± 2.1% | -9.3 ± 5.2% |
| | 2011 – 2017 | -5.3 ± 6.0% | -4.3 ± 6.5% | -4.2 ± 3.0% | -4.9 ± 9.2% | -6.0 ± 1.8% | -3.8 ± 1.8% | -6.1 ± 25.6% | -3.8 ± 3.5% |
| OMI-NASA | 2005 – 2011 | -9.4 ± 5.0% | -9.6 ± 5.3% | -9.4 ± 2.8% | -7.1 ± 2.9% | -9.4 ± 3.2% | -8.1 ± 2.8% | -7.8 ± 3.6% | -9.5 ± 16.6% |
| | 2011 – 2016 | -4.4 ± 18.9% | -3.8 ± 7.5% | -5.7 ± 6.7% | -4.5 ± 5.3% | -6.0 ± 3.1% | -4.6 ± 3.9% | -12.8 ± 7.8% | -11.4 ± 6.6% |
| OMI-BEHR | 2005 – 2011 | -9.1 ± 5.3% | -8.9 ± 5.8% | -8.7 ± 2.4% | -6.4 ± 3.2% | -9.2 ± 3.2% | -8.0 ± 3.1% | -8.5 ± 10.6% | -9.4 ± 23.0% |
| | 2011 – 2016 | -3.8 ± 4.4% | -3.0 ± 4.0% | -5.4 ± 7.0% | -3.9 ± 6.6% | -5.6 ± 13.2% | -4.1 ± 14.0% | -9.9 ± 5.2% | -6.7 ± 5.9% |
| EPA | 2003 – 2011 | | | | | -6.5 ± 0.8% | | | |
| | 2011 – 2017 | | | | | -5.1 ± 0.3% | | | |

681

¹ We calculate trends by using the exponential model described in Table 1.

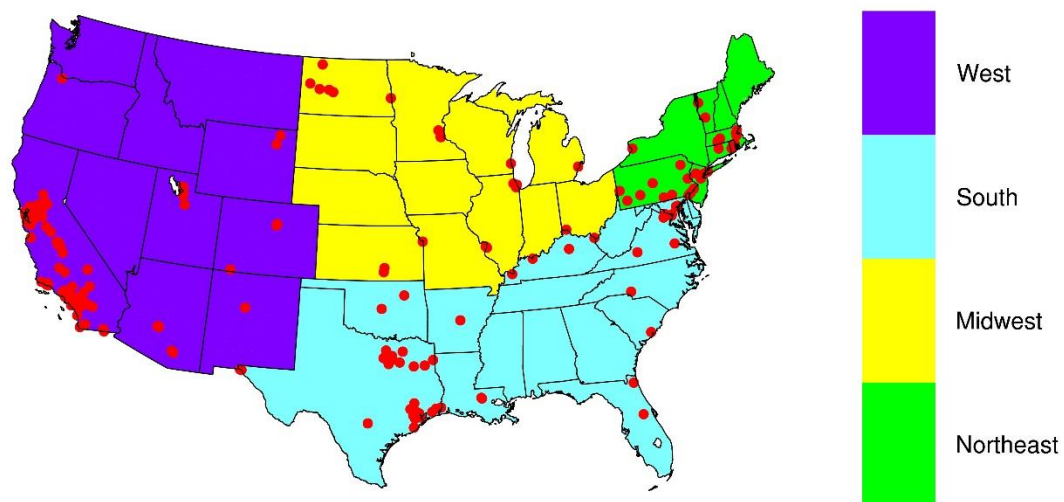


Figure 1. Region definitions and locations of NO₂ surface observation sites used in this study.

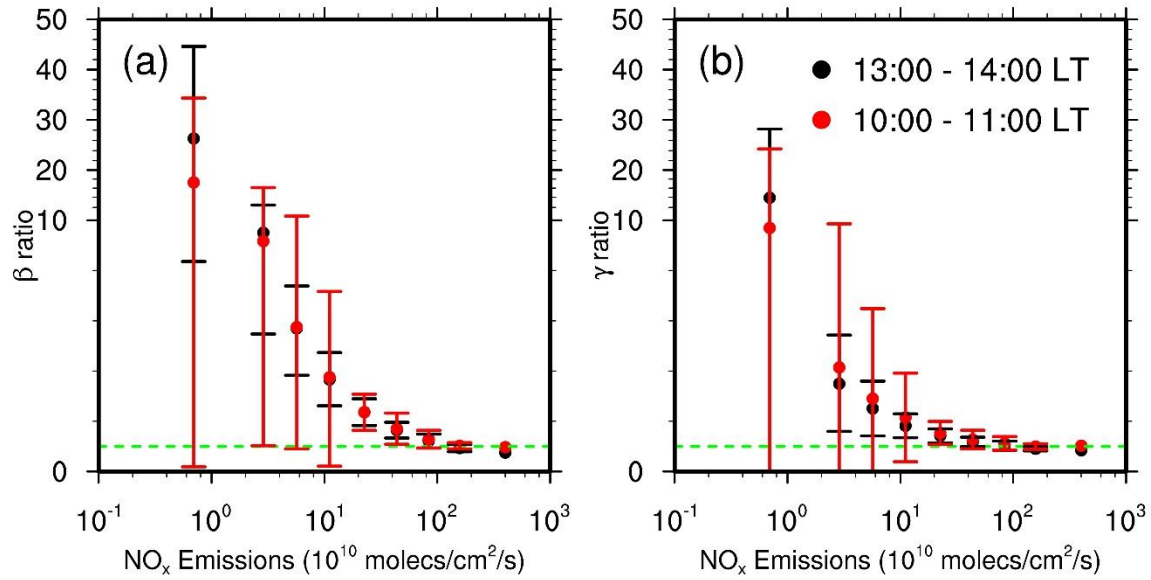


Figure 2. Distributions of β (panel a) and γ (panel b) ratios as a function of anthropogenic NO_x emissions on weekdays for July 2011 over the CONUS. “13:00 – 14:00 LT” is for OMI, and “10:00 – 11:00” LT is for SCIAMACHY and GOME-2A/2B. The data are binned into nine groups based on anthropogenic NO_x emissions: $E \in (0, 2^1), [2^1, 2^2), [2^2, 2^3), [2^3, 2^4), [2^4, 2^5), [2^5, 2^6), [2^6, 2^7), [2^7, 2^8), [2^8, 2^9) \times 10^{10}$ molecules $\text{cm}^{-2} \text{s}^{-1}$. Here, $(0, 2^1)$ denotes $0 < \text{emissions} < 2^1$, and $[2^1, 2^2)$ denotes $2^1 \leq \text{emissions} < 2^2$, similar to other intervals. The green dashed line denotes a value of 1. Error bars denote standard deviations.

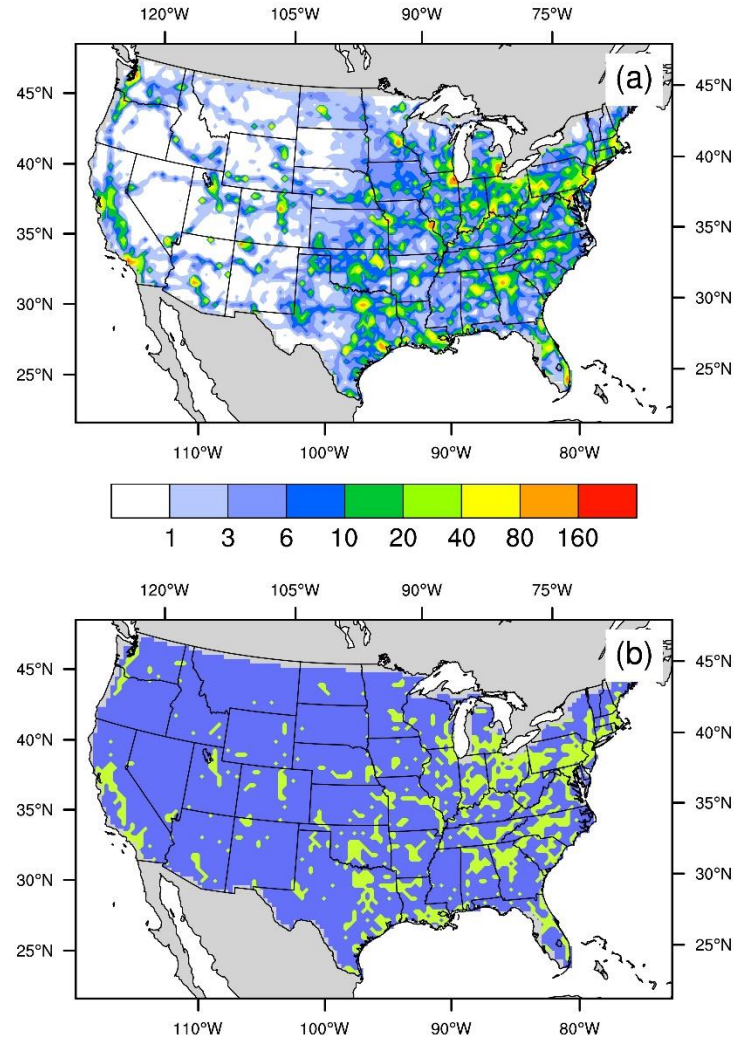


Figure 3. Spatial distributions of (a) anthropogenic NO_x emissions (unit: 10¹⁰ molecules cm⁻² s⁻¹) and (b) “urban” regions satisfying our selection criteria. In (b), light green and blue denote the resulting urban and rural regions, respectively.

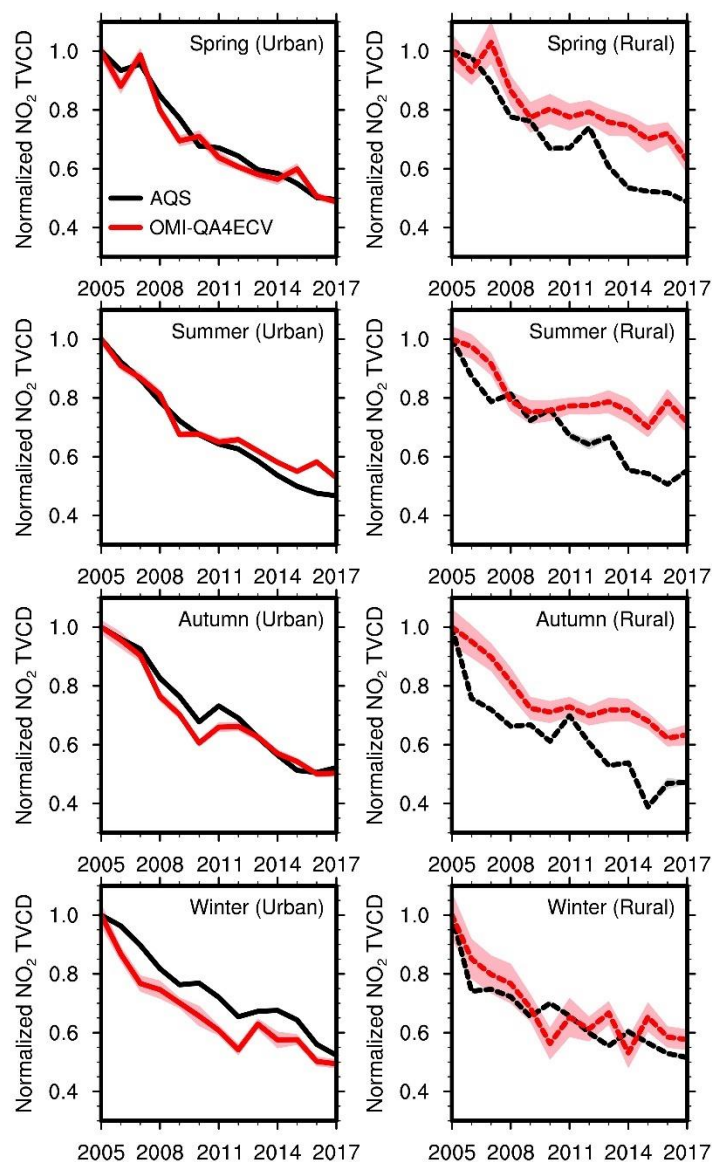


Figure 4. Relative annual variations of AQS NO₂ surface concentrations and coincident OMI-QA4ECV NO₂ TVCD in each season from 2005 – 2017 for urban (left panel) and rural (right panel) regions. The observation data are scaled by the corresponding 2005 values. Black and red lines denote AQS surface observations and OMI-QA4ECV NO₂ TVCDs, respectively. Shading in a lighter color is added to show the standard deviation of the results; when uncertainty is small due in part to a large number of data points, shading area may not show up.

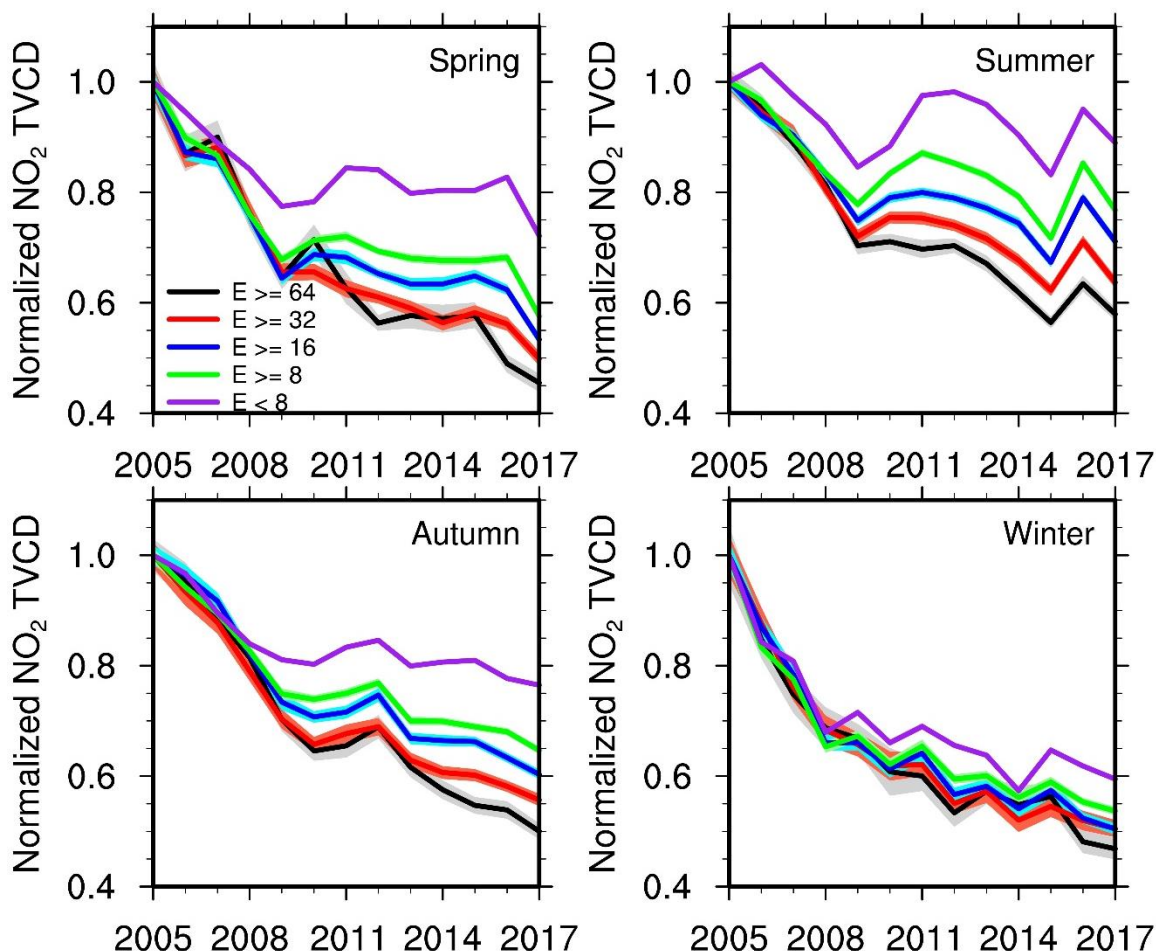


Figure 5. Relative annual variations of OMI-QA4ECV NO₂ TVCD for different anthropogenic NO_x-emission groups based on NEI2011 in each season from 2005 – 2017. “E ≥ 64” denotes grid cells with anthropogenic NO_x emissions over 64×10^{10} molecules cm⁻² s⁻¹. “E ≥ 32” denotes grid cells with anthropogenic NO_x emissions equal to or larger than 32×10^{10} molecules cm⁻² s⁻¹ but less than 64×10^{10} molecules cm⁻² s⁻¹. “E ≥ 16” and “E ≥ 8” have similar meanings as “E ≥ 32”. “E < 8” denotes grid cells with anthropogenic NO_x emissions less than 8×10^{10} molecules cm⁻² s⁻¹. Shading in a lighter color is added to show the standard deviation of the results; when uncertainty is small due in part to a large number of data points, shading area may not show up.

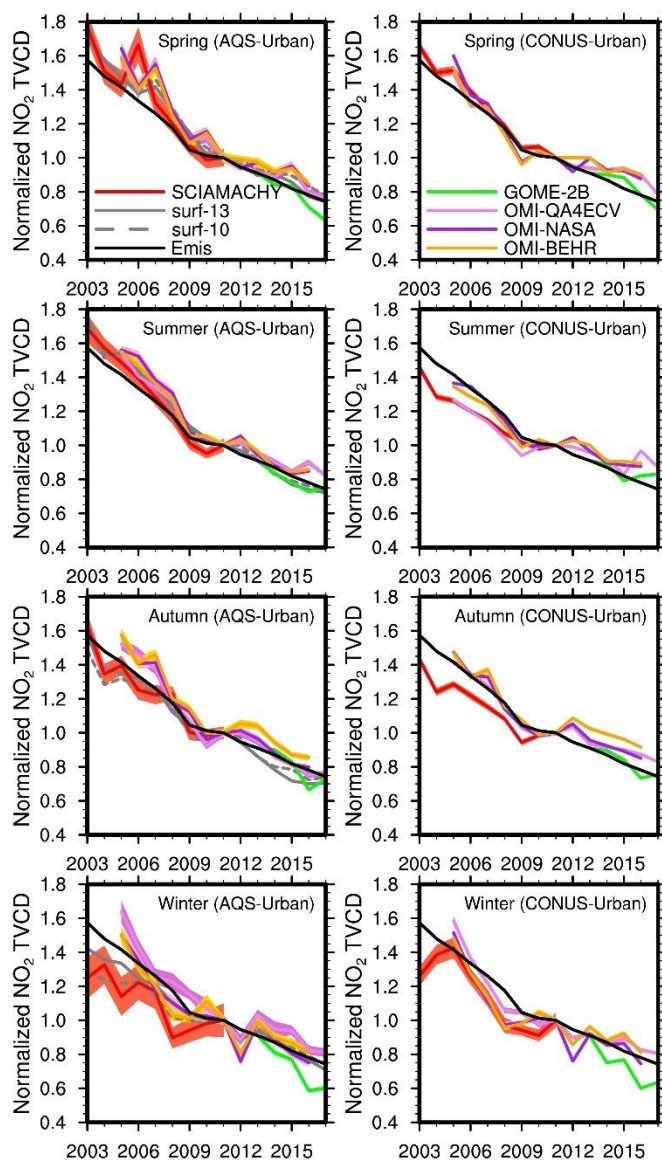


Figure 6. Relative variations of AQS NO₂ surface measurements at 13:00-14:00 and 10:00-11:00 LT, updated EPA anthropogenic NO_x emissions, and satellite NO₂ TVCD data over the AQS urban sites (left column) and the CONUS urban regions (right column) for 4 seasons. AQS NO₂ surface measurements are not included in the right column. All datasets are scaled by their corresponding values in 2011 except for GOME-2B. For GOME-2B, we firstly normalized the values in each season to the corresponding 2013 values and plotted the relative changes from the 2013 EPA point of each season to make the GOME-2B relative variations comparable to the other datasets. Shading in a lighter color is added to show the standard deviation of the results; when uncertainty is small due in part to a large number of data points, shading area may not show up.

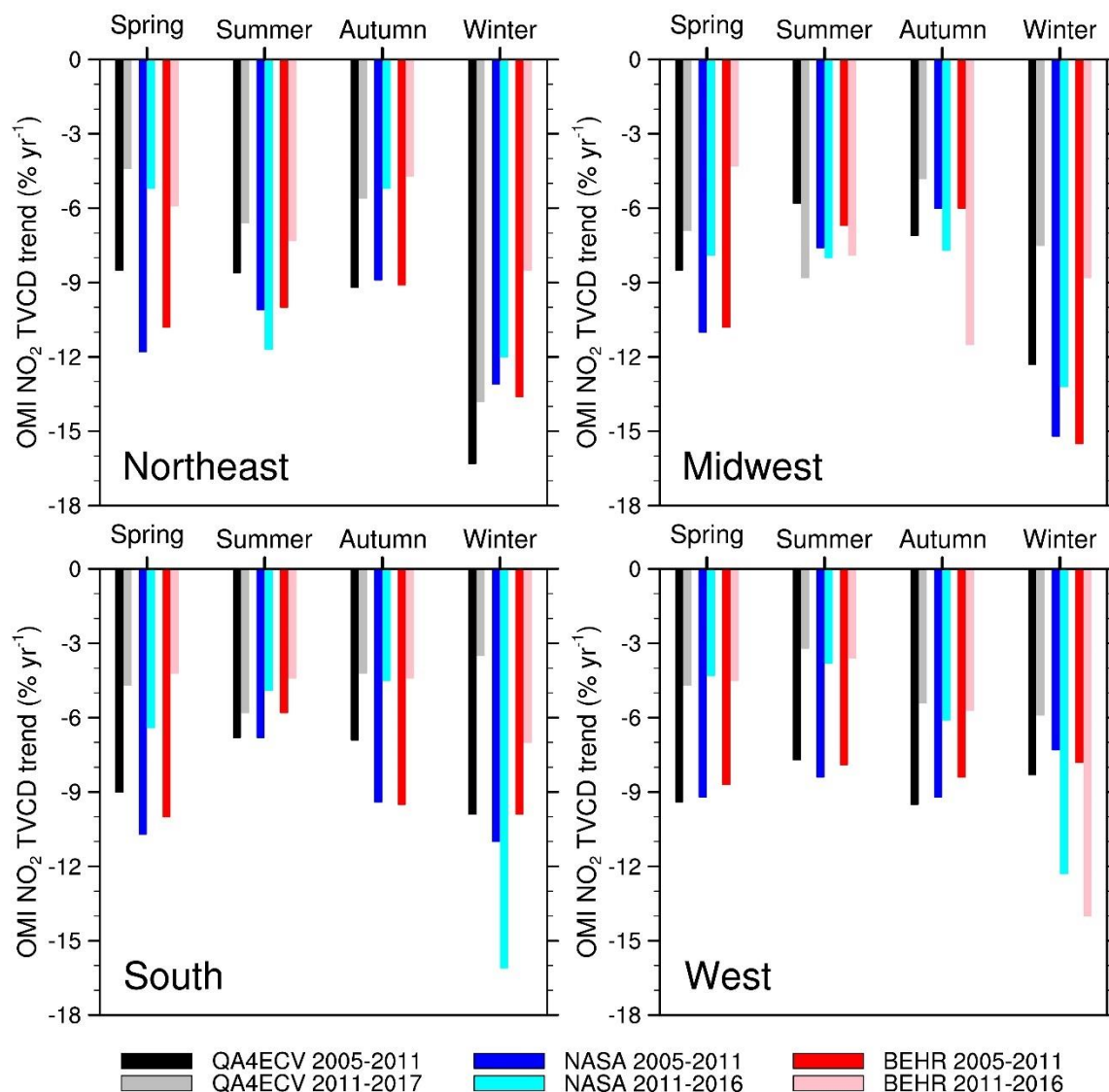


Figure 7. Pre- and post-2011 OMI NO₂ TVCD trends for 4 seasons in the urban regions of Northeast, Midwest, South, and West. Black bars denote OMI-QA4ECV NO₂ TVCD trends from 2005 – 2011; gray bars denote the corresponding trends during 2011 – 2017. Blue bars denote OMI-NASA trends from 2005 – 2011; cyan bars denote NASA-OMI trends from 2011 – 2016. Red bars denote BEHR-OMI trends from 2005 – 2011; pink bars denote OMI-BEHR trends from 2011 – 2016.

Inferring the anthropogenic NO_x emission trend over the United States during 2003 - 2017 from satellite observations: Was there a flattening of the emission trend after the Great Recession?

Jianfeng Li^{1,[a](#)}, Yuhang Wang^{1*}

¹School of Earth and Atmospheric Sciences, Georgia Institute of Technology, Atlanta, Georgia, USA

^a [Now at Pacific Northwest National Laboratory, Richland, WA, USA](#)

* *Correspondence to* Yuhang Wang (yuhang.wang@eas.gatech.edu)

13 **Table Captions**

14 Table S1. Summary of major satellite instruments for remote sensing of atmospheric NO₂ VCD in
15 the past decade

16 Table S2. Summary of satellite NO₂ TVCD products and their retrieval information

17 Table S3. Selection criteria for satellite NO₂ TVCD pixel data

18 Table S4. Summary of annual trends of AQS NO₂ surface concentrations and satellite NO₂ TVCD
19 products in each region during different periods

20 **Table S1. Summary of major satellite instruments for remote sensing of atmospheric NO₂ VCD in the past decade**

| Instrument | Satellite | Launch date | End date | Operator | Equator crossing time (local time) | UV/Vis Spectral range (nm) | Spectral resolution (nm) | Swath length (km) | Nadir pixel resolution (km × km) | Global coverage (days) |
|------------|------------------------|-------------------------|-------------------------|-----------------------|------------------------------------|----------------------------|--------------------------|---|--|------------------------|
| SCIAMACHY | ENVISAT ¹ | 03/01/2002 ² | 04/08/2012 ² | ESA ³ | 10:00 ¹ | 240 – 805 ⁴ | 0.24 – 0.48 ⁴ | 960 ⁵ | 60 × 30 ⁵ | 6 ⁵ |
| GOME-2A | MetOp-A ⁶ | 10/19/2006 ⁶ | in operation | EUMETSAT ⁷ | 9:30 ⁸ | 240 – 790 ⁸ | 0.26 – 0.51 ⁸ | 1920 before Jul. 15 th , 2013; 960 after Jul. 15 th , 2013 ⁸ | 80 × 40 before Jul. 15 th , 2013; 40 × 40 after Jul. 15 th , 2013 ⁸ | 1.5 ⁹ |
| GOME-2B | MetOp-B ⁶ | 09/17/2012 ⁶ | In operation | EUMETSAT | 9:30 ⁸ | 240 – 790 ⁸ | 0.26 – 0.51 ⁸ | 1920 ⁸ | 80 × 40 ⁸ | 1.5 ⁹ |
| OMI | EOS-Aura ¹⁰ | 07/152004 ¹⁰ | In operation | NASA | 13:45 ¹⁰ | 270 – 500 ¹¹ | 0.45 – 1.0 ¹¹ | 2600 ¹¹ | 24 × 13 ¹¹ | 1 ¹¹ |

21 ¹ Refer to <https://earth.esa.int/web/guest/missions/esa-operational-eo-missions/envisat>
22 ² Refer to <https://en.wikipedia.org/wiki/Envisat>
23 ³ The European Space Agency
24 ⁴ Refer to <http://www.iup.uni-bremen.de/sciamachy/instrument/performance/index.html>
25 ⁵ Refer to Boersma et al. (2008), Boersma et al. (2009), and Lee et al. (2009)
26 ⁶ Refer to <https://www.eumetsat.int/website/home/Satellites/CurrentSatellites/Metop/index.html>
27 ⁷ The European Organization for the Exploitation of Meteorological Satellites
28 ⁸ Refer to EUMETSAT (2015)
29 ⁹ Refer to Lee et al. (2009) and Wang et al. (2017)
30 ¹⁰ Refer to <https://aura.gsfc.nasa.gov/>
31 ¹¹ Refer to <https://aura.gsfc.nasa.gov/omi.html>

32 **Table S2. Summary of satellite NO₂ TVCD products and their retrieval information**

| NO ₂ TVCD products | Version | Available period | DOAS fitting method | Stratosphere–troposphere separation | Fitting window (nm) | Albedo / reflectance | A priori profiles | Radiative transfer model | Cloud | Uncertainty |
|-------------------------------|---------------|-------------------------|---|--|----------------------------|--|--------------------------------|--------------------------|---|--|
| GOME-2B | TM4NO2A (2.3) | 12/20/2012 – current | Intensity fit ¹ | Assimilation of satellite total slant columns in the TM4 model ^{2, 3} | 405 – 465 ¹ | Climatology albedo from 3 years of OMI data ⁴ | TM4 (2° × 3°) ² | DAK ² | FRESCO+ (Oxygen A-band around 760 nm) ⁵ | 1.0 × 10 ¹⁵ molecules/cm ² + 25% ² |
| SCIAMACHY | QA4ECV (v1.1) | 08/02/2002 – 04/08/2012 | Optical Density ^{1, 6} | Assimilation of OMI total slant columns in the TM5 - MP model ^{6, 7} | 425 – 465 ⁶ | Climatology albedo based on SCIAMACHY ⁸ | TM5-MP (1° × 1°) ⁶ | DAK | FRESCO+ | 35% - 45% over polluted scenes; > 100% over background regions (Pacific Ocean) ⁶ |
| GOME-2A | QA4ECV (v1.1) | 02/01/2007 – 12/31/2016 | | | 405 – 465 ^{1, 6} | Climatology albedo based on GOME-2A ⁸ | | | FRESCO+ | |
| OMI-QA4ECV | QA4ECV (v1.1) | 10/012004 – Current | | | 405 – 465 ^{1, 6} | Climatology albedo from 5 years of OMI data ⁶ | | | Improved O ₂ -O ₂ (477 nm) ⁹ | |
| OMI-NASA | SPv3 | 01/01/2005 – 07/31/2017 | | | 402 – 465 ^{1, 10} | OMI climatology albedo ¹⁰ | GMI (1° × 1.25°) ¹⁰ | TMORAD ¹⁰ | O ₂ -O ₂ (477 nm) ^{10, 11} | SPv2.1 TVCD has uncertainties of about 30% under clear-sky conditions to about 60% under cloudy conditions ¹² , and the relative difference between SPv3 and SPv2.1 is less than ~20% ¹⁰ . |
| OMI-BEHR ¹³ | v3.0B | 01/01/2005 – 07/31/2017 | Stepwise intensity fit with monthly averaged solar irradiance spectrum ^{1, 10} | Based on OMI total slant columns over regions with low estimated TVCD contributions (TVCD contributions less than 0.3 × 10 ¹⁵ molecules/cm ²) ¹⁰ | | Based on MCD43D BRDF product (for land) and model parameterization (for ocean) | WRF-Chem (12 km) | | | |

33 ¹ Refer to Zara et al. (2018)

34 ² Refer to Boersma et al. (2011). “TM4” is the Tracer Model, version 4. “DAK” is the Doubling-Adding KNMI (DAK) radiative transfer model.

35 ³ Refer to Williams et al. (2009)

36 ⁴ Refer to Kleipool et al. (2008)

37 ⁵ Refer to Wang et al. (2017) and Wang et al. (2008)

38 ⁶ Refer to Boersma et al. (2018)

39 ⁷ Refer to Williams et al. (2017)

40 ⁸ Refer to Tilstra et al. (2017)

41 ⁹ Refer to Veeffkind et al. (2016)

42 ¹⁰ Refer to Bucsela et al. (2013), Bucsela et al. (2016), Krotkov et al. (2017), and Marchenko et al. (2015). “TMORAD” is the TMOS radiative transfer model.

43 ¹¹ Refer to Acarreta et al. (2004)

44 ¹² Refer to Lamsal et al. (2014), Oetjen et al. (2013), and Tong et al. (2015)

45 ¹³ Refer to Laughner et al. (2018). OMI-BEHR uses the SCD from OMI-NASA SPv3 but updates inputs for the AMF calculation, such as a prior NO₂ vertical profiles and surface reflectance. Besides, OMI-BEHR only provides NO₂ TVCD over the contiguous

46 United States (CONUS). As in this study, we used the OMI-NASA datasets archived in the OMI-BEHR product, so we only obtained OMI-NASA datasets extended to July 31, 2017.

47 ¹⁴ Average uncertainty over the CONUS is calculated based on the file from <http://behr.cchem.berkeley.edu/behr/BEHR-us-uncertainty.hdf>

48 **Table S3. Selection criteria for satellite NO₂ TVCD pixel data**

| NO ₂ TVCD products | Period | Solar zenith angle | albedo | Cloud radiance fraction | Snow or ice covered | AMFtrop/AMFgeo | Flag for retrieval success | Retrieval quality flag | Rows in swath |
|-------------------------------|-------------------------|--------------------|--------|-------------------------|---------------------|----------------|----------------------------|------------------------|---------------|
| GOME-2B | 01/01/2013 – 12/31/2017 | < 80° | <= 0.3 | <= 50% | No | > 0.2 | Yes | | All |
| SCIAMACHY | 01/01/2003 – 12/31/2011 | < 80° | <= 0.3 | <= 50% | No | > 0.2 | Yes | | All |
| GOME-2A | 01/01/2008 – 12/31/2016 | < 80° | <= 0.3 | <= 50% | No | > 0.2 | Yes | | All |
| OMI-QA4ECV ¹ | 01/01/2005 – 12/31/2017 | < 80° | <= 0.3 | <= 50% | No | > 0.2 | Yes | | 6 - 21 |
| OMI-NASA ¹ | 01/01/2005 – 12/31/2016 | < 80° | <= 0.3 | <= 50% | | | Yes | Yes | 6 – 21 |
| OMI-BEHR ¹ | 01/01/2005 – 12/31/2016 | < 80° | <= 0.3 | <= 50% | | | Yes | Yes | 6 - 21 |

49 ¹ Rows 6-21 are selected to remove the anomalies developed in the OMI sensor (Boersma et al., 2018; Zhang et al., 2018).

50 **Table S4. Summary of annual trends of AQS NO₂ surface concentrations and satellite NO₂ TVCD products in each region during different periods¹**

| | | Northeast | | Midwest | | South | | West | |
|---|-------------|---------------|--------------|---------------|--------------|--------------|-------------|---------------|--------------|
| | | AQS site | CONUS | AQS site | CONUS | AQS site | CONUS | AQS site | CONUS |
| AQS NO ₂ VMR at 13:00 -14:00 | 2003 – 2011 | -6.8 ± 0.7% | | -6.1 ± 1.2% | | -6.6 ± 0.7% | | -7.6 ± 1.2% | |
| | 2011 – 2017 | -8.0 ± 1.2% | | -6.4 ± 0.8% | | -5.8 ± 0.6% | | -7.2 ± 1.6% | |
| AQS NO ₂ VMR at 10:00 – 11:00 | 2003 – 2011 | -6.6 ± 0.5% | | -5.8 ± 1.5% | | -6.5 ± 1.3% | | -7.1 ± 1.6% | |
| | 2011 – 2017 | -7.6 ± 1.0% | | -6.8 ± 0.5% | | -5.7 ± 0.1% | | -6.1 ± 1.1% | |
| SCIAMACHY | 2003 – 2011 | -17.1 ± 2.7% | -11.0 ± 3.3% | -12.9 ± 6.8% | -6.5 ± 0.8% | -9.1 ± 1.0% | -6.2 ± 1.5% | -9.1 ± 1.8% | -7.0 ± 1.4% |
| | 2011 – 2017 | | | | | | | | |
| GOME2B | 2003 – 2011 | | | | | | | | |
| | 2013 – 2017 | -11.4 ± 3.7% | -10.8 ± 3.9% | -9.9 ± 13.1% | -4.4 ± 27.2% | -8.9 ± 3.0% | -7.5 ± 3.6% | -11.8 ± 3.0% | -10.6 ± 2.3% |
| OMI-QA4ECV | 2005 – 2011 | -14.2 ± 6.3% | -10.6 ± 3.8% | -9.2 ± 4.2% | -8.4 ± 2.8% | -9.2 ± 2.7% | -8.2 ± 1.5% | -10.5 ± 1.6% | -8.7 ± 0.9% |
| | 2011 – 2017 | -18.0 ± 16.2% | -7.6 ± 4.2% | -7.6 ± 3.3% | -7.0 ± 1.7% | -4.8 ± 1.4% | -4.6 ± 1.0% | -6.4 ± 1.4% | -4.8 ± 1.2% |
| OMI-NASA | 2005 – 2011 | -11.8 ± 1.3% | -11.0 ± 1.8% | -10.9 ± 4.8% | -10.0 ± 4.1% | -10.0 ± 3.5% | -9.5 ± 1.9% | -10.2 ± 1.8% | -8.5 ± 0.9% |
| | 2011 – 2016 | -10.0 ± 4.9% | -8.5 ± 3.8% | -13.2 ± 3.2% | -9.2 ± 2.7% | 0.3 ± 19.2% | -8.0 ± 5.5% | -9.0 ± 5.7% | -6.6 ± 3.9% |
| OMI-BEHR | 2005 – 2011 | -11.8 ± 1.8% | -10.9 ± 1.9% | -12.2 ± 7.3% | -9.8 ± 4.4% | -9.5 ± 3.1% | -8.8 ± 2.0% | -9.9 ± 1.1% | -8.2 ± 0.4% |
| | 2011 – 2016 | -8.2 ± 3.4% | -6.6 ± 1.7% | -27.4 ± 24.3% | -8.1 ± 3.0% | -7.2 ± 2.3% | -5.0 ± 1.3% | -13.2 ± 14.5% | -7.0 ± 4.8% |

51 ¹ Annual trends are the averages of regional seasonal trends (e.g, Figure 7).

52

53 **References**

- 54 Acarreta, J. R., de Haan, J. F., and Stammes, P.: Cloud pressure retrieval using the O₂-O₂
55 absorption band at 477 nm, *J. Geophys. Res.-Atmos.*, 109,
56 <https://doi.org/10.1029/2003JD003915>, 2004.
- 57 Boersma, K. F., Jacob, D. J., Eskes, H. J., Pinder, R. W., Wang, J., and Van Der A, R. J.:
58 Intercomparison of SCIAMACHY and OMI tropospheric NO₂ columns: Observing the diurnal
59 evolution of chemistry and emissions from space, *J. Geophys. Res.-Atmos.*, 113,
60 <https://doi.org/10.1029/2007JD008816>, 2008.
- 61 Boersma, K. F., Jacob, D. J., Trainic, M., Rudich, Y., De Smedt, I., Dirksen, R., and Eskes, H. J.:
62 Validation of urban NO₂ concentrations and their diurnal and seasonal variations observed from
63 the SCIAMACHY and OMI sensors using in situ surface measurements in Israeli cities, *Atmos.*
64 *Chem. Phys.*, 9, 3867-3879, <https://doi.org/10.5194/acp-9-3867-2009>, 2009.
- 65 Boersma, K. F., Eskes, H. J., Dirksen, R. J., Veefkind, J. P., Stammes, P., Huijnen, V., Kleipool,
66 Q. L., Sneep, M., Claas, J., and Leitão, J.: An improved tropospheric NO₂ column retrieval
67 algorithm for the Ozone Monitoring Instrument, *Atmos. Meas. Tech.*, 4, 1905-1928,
68 <https://doi.org/10.5194/amt-4-1905-2011>, 2011.
- 69 Boersma, K. F., Eskes, H. J., Richter, A., De Smedt, I., Lorente, A., Beirle, S., van Geffen, J. H.,
70 Zara, M., Peters, E., and Roozendael, M. V.: Improving algorithms and uncertainty estimates for
71 satellite NO₂ retrievals: results from the quality assurance for the essential climate variables
72 (QA4ECV) project, *Atmos. Meas. Tech.*, 11, 6651-6678, [https://doi.org/10.5194/amt-11-6651-](https://doi.org/10.5194/amt-11-6651-2018)
73 2018, 2018.
- 74 Bucsela, E. J., Krotkov, N. A., Celarier, E. A., Lamsal, L. N., Swartz, W. H., Bhartia, P. K.,
75 Boersma, K. F., Veefkind, J. P., Gleason, J. F., and Pickering, K. E.: A new stratospheric and
76 tropospheric NO₂ retrieval algorithm for nadir-viewing satellite instruments: applications to OMI,
77 *Atmos. Meas. Tech.*, 6, 2607-2626, <https://doi.org/10.5194/amt-6-2607-2013>, 2013.
- 78 Bucsela, E. J., Celarier, E. A., Gleason, J. L., Krotkov, N. A., Lamsal, L. N., Marchenko, S. V.,
79 and Swartz, W. H.: OMNO2 README Document Data Product Version 3.0, NASA, 38, 2016.
- 80 EUMETSAT: GOME_FACTSHEET, Germany, 33, 2015.
- 81 Kleipool, Q. L., Dobber, M. R., de Haan, J. F., and Levelt, P. F.: Earth surface reflectance
82 climatology from 3 years of OMI data, *J. Geophys. Res.-Atmos.*, 113,
83 <https://doi.org/10.1029/2008JD010290>, 2008.
- 84 Krotkov, N. A., Lamsal, L. N., Celarier, E. A., Swartz, W. H., Marchenko, S. V., Bucsela, E. J.,
85 Chan, K. L., Wenig, M., and Zara, M.: The version 3 OMI NO₂ standard product, *Atmos. Meas.*
86 *Tech.*, 10, 3133-3149, <https://doi.org/10.5194/amt-10-3133-2017>, 2017.
- 87 Lamsal, L. N., Krotkov, N. A., Celarier, E. A., Swartz, W. H., Pickering, K. E., Bucsela, E. J.,
88 Gleason, J. F., Martin, R. V., Philip, S., and Irie, H.: Evaluation of OMI operational standard NO₂

89 column retrievals using in situ and surface-based NO₂ observations, *Atmos. Chem. Phys.*, 14,
90 11587-11609, <https://doi.org/10.5194/acp-14-11587-2014>, 2014.

91 Laughner, J. L., Zhu, Q., and Cohen, R. C.: The Berkeley High Resolution Tropospheric NO₂
92 product, *Earth System Science Data*, 10, 2069-2095, <https://doi.org/10.5194/essd-10-2069-2018>,
93 2018.

94 Lee, C., Martin, R. V., van Donkelaar, A., Richter, A., Burrows, J. P., and Kim, Y. J.: Remote
95 Sensing of Tropospheric Trace Gases (NO₂ and SO₂) from SCIAMACHY, in: *Atmospheric and*
96 *Biological Environmental Monitoring*, Springer, 63-72, 2009.

97 Marchenko, S., Krotkov, N. A., Lamsal, L. N., Celarier, E. A., Swartz, W. H., and Bucsela, E. J.:
98 Revising the slant column density retrieval of nitrogen dioxide observed by the Ozone
99 Monitoring Instrument, *J. Geophys. Res.-Atmos.*, 120, 5670-5692,
100 <https://doi.org/10.1002/2014JD022913>, 2015.

101 Oetjen, H., Baidar, S., Krotkov, N. A., Lamsal, L. N., Lechner, M., and Volkamer, R.: Airborne
102 MAX-DOAS measurements over California: Testing the NASA OMI tropospheric NO₂ product,
103 *J. Geophys. Res.-Atmos.*, 118, 7400-7413, <https://doi.org/10.1002/jgrd.50550>, 2013.

104 Tilstra, L. G., Tuinder, O. N. E., Wang, P., and Stammes, P.: Surface reflectivity climatologies
105 from UV to NIR determined from Earth observations by GOME-2 and SCIAMACHY, *J.*
106 *Geophys. Res.-Atmos.*, 122, 4084-4111, <https://doi.org/10.1002/2016JD025940>, 2017.

107 Tong, D., Lamsal, L., Pan, L., Ding, C., Kim, H., Lee, P., Chai, T., Pickering, K. E., and Stajner,
108 I.: Long-term NO_x trends over large cities in the United States during the great recession:
109 Comparison of satellite retrievals, ground observations, and emission inventories, *Atmos.*
110 *Environ.*, 107, 70-84, <https://doi.org/10.1016/j.atmosenv.2015.01.035>, 2015.

111 Veefkind, J. P., de Haan, J. F., Sneep, M., and Levelt, P. F.: Improvements to the OMI O₂-O₂
112 operational cloud algorithm and comparisons with ground-based radar-lidar observations, *Atmos.*
113 *Meas. Tech.*, 9, 6035-6049, <https://doi.org/10.5194/amt-9-6035-2016>, 2016.

114 Wang, P., Stammes, P., van der A, R., Pinardi, G., and van Roozendael, M.: FRESCO+: an
115 improved O₂ A-band cloud retrieval algorithm for tropospheric trace gas retrievals, *Atmos.*
116 *Chem. Phys.*, 8, 6565-6576, <https://doi.org/10.5194/acp-8-6565-2008>, 2008.

117 Wang, Y., Beirle, S., Lampel, J., Koukouli, M., De Smedt, I., Theys, N., Ang, L., Wu, D., Xie, P.,
118 and Liu, C.: Validation of OMI, GOME-2A and GOME-2B tropospheric NO₂, SO₂ and HCHO
119 products using MAX-DOAS observations from 2011 to 2014 in Wuxi, China: investigation of the
120 effects of priori profiles and aerosols on the satellite products, *Atmos. Chem. Phys.*, 17, 5007,
121 <https://doi.org/10.5194/acp-17-5007-2017>, 2017.

122 Williams, J. E., Scheele, M. P., van Velthoven, P. F. J., Cammas, J.-P., Thouret, V., Galy-Lacaux,
123 C., and Volz-Thomas, A.: The influence of biogenic emissions from Africa on tropical
124 tropospheric ozone during 2006: a global modeling study, *Atmos. Chem. Phys.*, 9, 5729-5749,
125 <https://doi.org/10.5194/acp-9-5729-2009>, 2009.

126 Williams, J. E., Boersma, K. F., Sager, P. L., and Verstraeten, W. W.: The high-resolution version
127 of TM5-MP for optimized satellite retrievals: description and validation, *Geoscientific Model*
128 *Development*, 10, 721-750, <https://doi.org/10.5194/gmd-10-721-2017>, 2017.

129 Zara, M., Boersma, K. F., De Smedt, I., Richter, A., Peters, E., Van Geffen, J. H. G. M., Beirle,
130 S., Wagner, T., Van Roozendaal, M., and Marchenko, S.: Improved slant column density retrieval
131 of nitrogen dioxide and formaldehyde for OMI and GOME-2A from QA4ECV: intercomparison,
132 uncertainty characterization, and trends, *Meas. Tech. Discuss.*, 1-47, [https://doi.org/10.5194/amt-](https://doi.org/10.5194/amt-11-4033-2018)
133 [11-4033-2018](https://doi.org/10.5194/amt-11-4033-2018), 2018.

134 Zhang, R., Wang, Y., Smeltzer, C., Qu, H., Koshak, W., and Boersma, K. F.: Comparing OMI-
135 based and EPA AQS in situ NO₂ trends: towards understanding surface NO_x emission changes,
136 *Atmos. Meas. Tech.*, 11, 3955-3967, <https://doi.org/10.5194/amt-11-3955-2018>, 2018.

137

Inferring the anthropogenic NO_x emission trend over the United States during 2003 - 2017 from satellite observations: Was there a flattening of the emission trend after the Great Recession?

Jianfeng Li^{1,[a](#)}, Yuhang Wang^{1*}

¹School of Earth and Atmospheric Sciences, Georgia Institute of Technology, Atlanta, Georgia, USA

^a [Now at Pacific Northwest National Laboratory, Richland, WA, USA](#)

* *Correspondence to* Yuhang Wang (yuhang.wang@eas.gatech.edu)

Figure Captions

Figure S1. Annual variation of NO_3^- wet deposition fluxes for each season from 2003 – 2017. The fluxes were scaled by the corresponding values in 2003. Shaded regions denote standard deviations. Monthly NO_3^- wet deposition observations are obtained from <https://nadp.slh.wisc.edu/data/NTN/ntnAllsites.aspx> (last access, September 29, 2019).

Figure S2. Comparison between original EPA anthropogenic NO_x emissions and updated EPA anthropogenic NO_x emissions with the newest Continuous Emission Monitoring Systems (CEMS) measurements.

Figure S3. Daily OMI NO_2 TVCDs for July 2011 (a) and 2012 (b) in Atlanta (33.755° N , 84.39° W). Black circles are weekday values, and red circles are weekend values. We find significant daily variations of NO_2 TVCD from (a) and (b). The number of available measurements in July 2011 is much less than July 2012. We find clear larger NO_2 TVCD values on weekdays than on weekends in July 2011, but the difference between weekday and weekend TVCDs in July 2012 are not so obvious.

Figure S4. Hourly averaged ratios of FEM (a) and CAPS (b) to FRM NO_2 measurements in each season, respectively. The FEM/FRM ratios are computed from coincident FRM and FEM measurements from 2013 – 2015 at 4 sites. The CAPS/FRM ratios are calculated based on coincident CAPS and FRM data from 2015 – 2016 at 3 sites.

Figure S5. Annual variations of AQS NO_2 surface concentrations at different hours on weekdays in spring (a, b), summer (c, d), autumn (e, f), and winter (g, h). Left panels show absolute NO_2 concentrations, and right panels are their relative variations normalized to 2011. To conduct reliable and consistent comparisons, we only used monitoring sites satisfying the seasonal $RCI < 50\%$ and continuity criteria on weekdays from 2003 – 2017.

Figure S6. Distributions of (a) NO₂ TVCD fraction that is in the boundary layer (< 2810 m) at 13:00 – 14:00, (b) NO₂ TVCD fraction in the boundary layer (< 1290 m) at 10:00 – 11:00, (c) the fraction of soil NO_x emissions in all surface sources (anthropogenic + soil) on weekdays for July 2011. As the lifetime of NO₂ in the free troposphere (several days ~ 2 weeks) is much longer than that in the boundary layer (~ 10 hours), local lightning NO_x emissions cannot represent NO₂ VCDs in the free troposphere. In this study, we apply NO₂ VCD in the free troposphere to analyze the impact of lightning NO_x on the nonlinear relationships between anthropogenic NO_x emissions and NO₂ TVCDs and use lightning NO_x and NO₂ VCD in the free troposphere interchangeably in the following.

Figure S7. (a) Distributions of the fractions of surface NO_x emissions emitted by soil (“SoilNO_x”), the portions of NO₂ TVCDs in the boundary layer (“PBLVCD”), and the fractions of NO₂ TVCDs from anthropogenic NO_x emissions (“AnthroVCD”) as functions of NEI2011 anthropogenic NO_x emissions at 13:00 – 14:00 LT on weekdays for July 2011 over the CONUS.

The fraction of NO₂ TVCDs from anthropogenic NO_x emissions is equal to $\left(1 - \right.$

$$\frac{E_{soil}}{E_{soil} + E_{anthropogenic}} \times \left(\frac{TVCD_{boundary}}{TVCD_{boundary} + TVCD_{free}} \right), \text{ where } E_{soil} \text{ denotes soil NO}_x \text{ emissions,}$$

$E_{anthropogenic}$ denotes anthropogenic NO_x emissions, $TVCD_{boundary}$ denotes NO₂ TVCDs in the boundary layer, and $TVCD_{free}$ denotes NO₂ TVCDs in the free troposphere. The calculated data are grouped into 9 bins as in Figure 2. (b) Same as (a), but for 10:00 – 11:00 LT. (c) Distributions of β_{Emis} , γ_{Emis} , β , and γ as functions of anthropogenic NO_x emissions at 13:00 – 14:00 LT on weekdays for July 2011 over the CONUS. β and γ are the same as Figure 2. β_{Emis} and γ_{Emis} denote β and γ values when no other factors are taken into consideration except for soil NO_x emissions, anthropogenic NO_x emissions, and NO₂ in the free troposphere. $\beta_{Emis} =$

$$\frac{15\%}{15\% \times \left(\frac{E_{anthropogenic}}{E_{anthropogenic} + E_{soil}} \right) \left(\frac{TVCD_{boundary}}{TVCD_{boundary} + TVCD_{free}} \right)} = \left(\frac{E_{anthropogenic} + E_{soil}}{E_{anthropogenic}} \right) \left(\frac{TVCD_{boundary} + TVCD_{free}}{TVCD_{boundary}} \right),$$

59 and $\gamma_{Emis} = \frac{15\%}{15\% \times \left(\frac{E_{anthropogenic}}{E_{anthropogenic} + E_{soil}} \right)} = \left(\frac{E_{anthropogenic} + E_{soil}}{E_{anthropogenic}} \right)$. It is noteworthy that here we

60 assume no interactions between the boundary layer and the free troposphere, boundary-layer NO_x

61 are only related to soil and anthropogenic NO_x emissions, and lightning NO_x only affect NO_2 in

62 the free troposphere. The assumptions are reasonable as the time scale (~ 1 week) of the

63 interactions between the boundary layer and the free troposphere ~~are-is~~ much longer than NO_x

64 lifetime in the boundary layer, and ~~in this study,~~ only a small fraction of lightning NO_x is

65 distributed into the boundary layer in this study. Therefore, β_{Emis} and γ_{Emis} roughly represent the

66 contributions of background sources (lightning NO_x and soil NO_x) to β and γ values. The

67 differences between β (γ) and β_{Emis} (γ_{Emis}) indicate the contribution of non-emission factors to β

68 (γ) values, such as chemistry, transport, NO_2 hydrolysis on aerosols, and dry ~~and wet~~ depositions.

69 (d) Same as (c), but for 10:00 – 11:00 LT. From (c) and (d)~~this figure~~, we find that both

70 background sources (lightning NO_x + soil NO_x) and non-emission factors are important when

71 considering the nonlinear relationships among NO_x emissions, NO_2 surface concentrations, and

72 NO_2 TVCDs in low-anthropogenic- NO_x emission regions. (e) Distribution of NO_x chemical

73 lifetimes as functions of anthropogenic NO_x emissions at 11:00 – 14:00 LT on weekdays for July

74 2011 over the CONUS. “Standard_surf” denotes NO_x chemical lifetimes at the surface layer from

75 the standard REAM simulation (“group 1” in Section 3.1); “Standard_trop” denotes average NO_x

76 chemical lifetimes in the troposphere for “group 1”; “Reduce_surf” denotes NO_x chemical

77 lifetimes at the surface layer for “group 2” with anthropogenic NO_x emissions reduced by 15%;

78 “Reduce_trop” denotes average NO_x chemical lifetimes in the troposphere for “group 2”. In this

79 study, we used the lifetimes at 11:00 – 14:00 LT but not 13:00 – 14:00 LT to partly include the

80 accumulation effect of NO_x emissions: NO_2 TVCD and NO_2 surface concentrations at 13:00 –

81 14:00 LT are not only affected by NO_x emissions at 13:00 – 14:00 LT but also by NO_x emissions

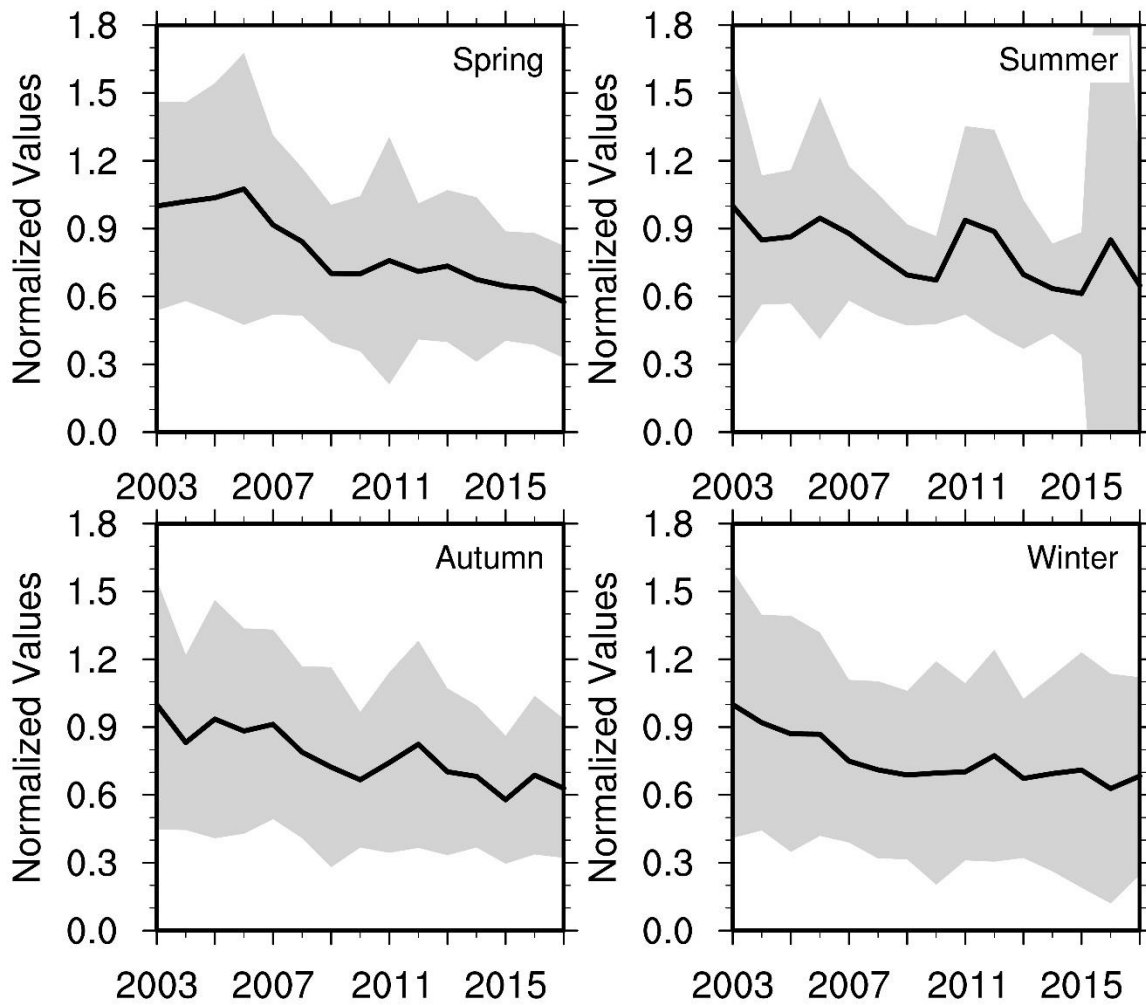
82 before that due to the NO_x chemical lifetime of several hours in daytime. (f) Same as (e), but for

83 8:00 – 11:00 LT. (g) Relative changes of NO_x chemical lifetimes at 11:00 – 14:00 LT on

weekdays for July 2011 over the CONUS due to the 15% decrease of anthropogenic NO_x emissions in “group 2”. “Surface” denotes the relative changes of NO_x chemical lifetimes at the surface, while “Troposphere” denotes the relative changes of average NO_x chemical lifetimes in the troposphere. We first calculated the relative changes in each grid cell via $\frac{lifetime_{Reduce}}{lifetime_{Standard}} - 1$, and then binned the calculated data into 9 groups as Figure 2. (h) Same as (g), but for 8:00 – 11:00 LT. In the chemical lifetime calculation, we included sinks from the reaction of OH + NO₂ and net losses due to organic nitrate production from the reactions of RO₂ with NO or NO₂ except for peroxyacyl nitrates (PANs), because PANs can be either a source or sink of NO_x depending on transport and chemistry. Only accounting for the sink from the reaction of OH + NO₂ produces significant different lifetimes in low-anthropogenic-NO_x emission bins and has less impact on high-anthropogenic-NO_x emission regions, which, however, does not affect our conclusions derived from subpanels (g) and (h) (the mean relative differences of chemical lifetimes between “group 1” and “group 2” are still < 10% in all bins): the chemical nonlinearity contributes little to β and γ values in low-anthropogenic-NO_x emission regions. Although not shown here, the impacts of NO₂ hydrolysis and NO₂ dry deposition on β and γ values are even smaller than those of chemical nonlinearity. Therefore, the differences between β (γ) and β_{Emis} (γ_{Emis}) in low-anthropogenic-NO_x emission bins in (c) and (d) mainly indicate the contribution of transport to β (γ) values. Error bars in (a), (b), (g), and (h) denote standard deviations.

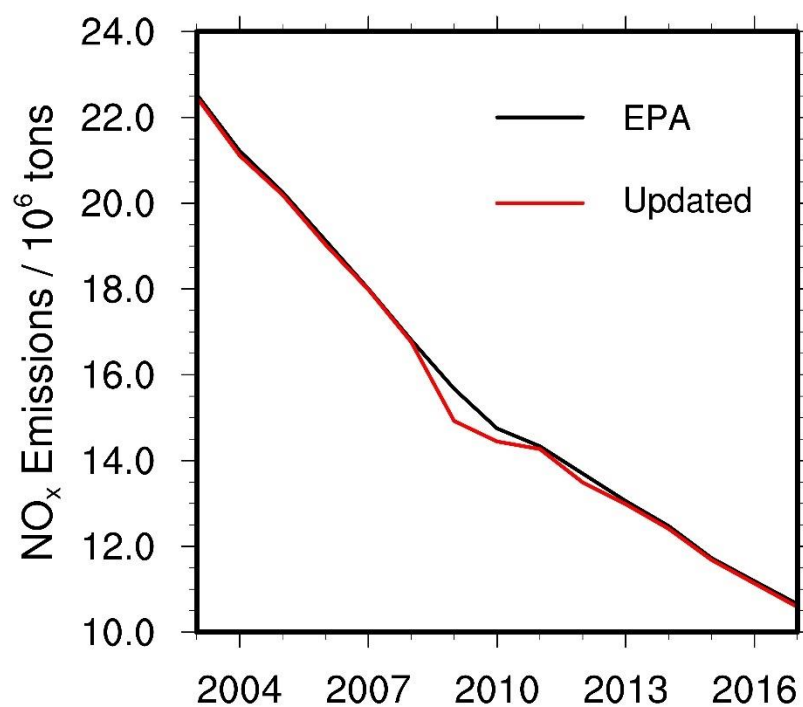
Figure S8. Same as Figure 4, but for AQS NO₂ surface concentrations and coincident GOME-2A NO₂ TVCD data during 2008 – 2016.

Figure S9. Relative variations of OMI-QA4ECV NO₂ TVCD data for urban regions (black lines) and the whole CONUS (red lines) from 2005 – 2017 in 4 seasons.



107

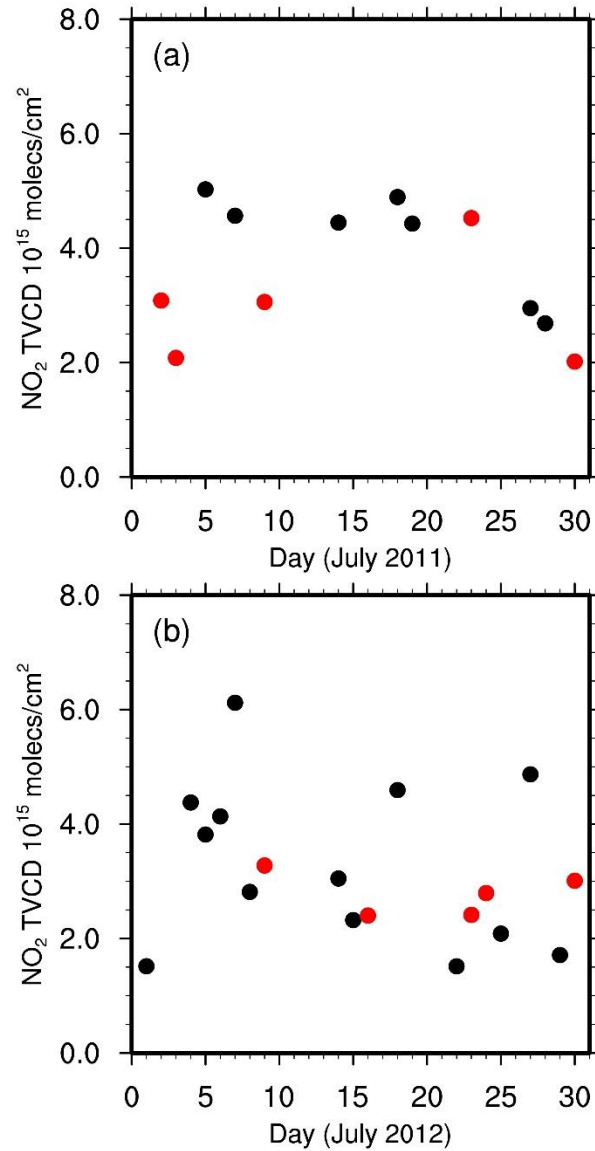
108 Figure S1. Annual variation of NO_3^- wet deposition fluxes for each season from 2003 – 2017. The
 109 fluxes were scaled by the corresponding values in 2003. Shaded regions denote standard
 110 deviations. Monthly NO_3^- wet deposition observations are obtained from
 111 <https://nadp.slh.wisc.edu/data/NTN/ntnAllsites.aspx> (last access, September 29, 2019).



112

113 Figure S2. Comparison between original EPA anthropogenic NO_x emissions and updated EPA
 114 anthropogenic NO_x emissions with the newest Continuous Emission Monitoring Systems
 115 (CEMS) measurements.

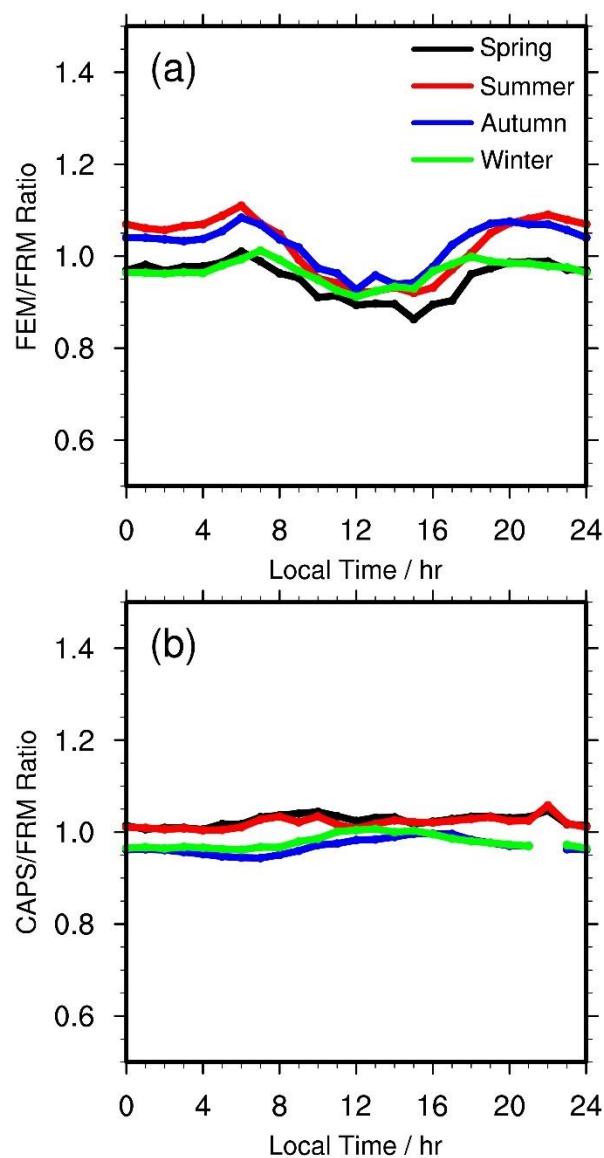
116



117

118 Figure S3. Daily OMI NO₂ TVCDs for July 2011 (a) and 2012 (b) in Atlanta (33.755° N, 84.39°
 119 W). Black circles are weekday values, and red circles are weekend values. We find significant
 120 daily variations of NO₂ TVCD from (a) and (b). The number of available measurements in July
 121 2011 is much less than July 2012. We find clear larger NO₂ TVCD values on weekdays than on
 122 weekends in July 2011, but the difference between weekday and weekend TVCDs in July 2012
 123 are not so obvious.

124



125

126 Figure S4. Hourly averaged ratios of FEM (a) and CAPS (b) to FRM NO_2 measurements in each
 127 season, respectively. The FEM/FRM ratios are computed from coincident FRM and FEM
 128 measurements from 2013 – 2015 at 4 sites. The CAPS/FRM ratios are calculated based on
 129 coincident CAPS and FRM data from 2015 – 2016 at 3 sites.

130

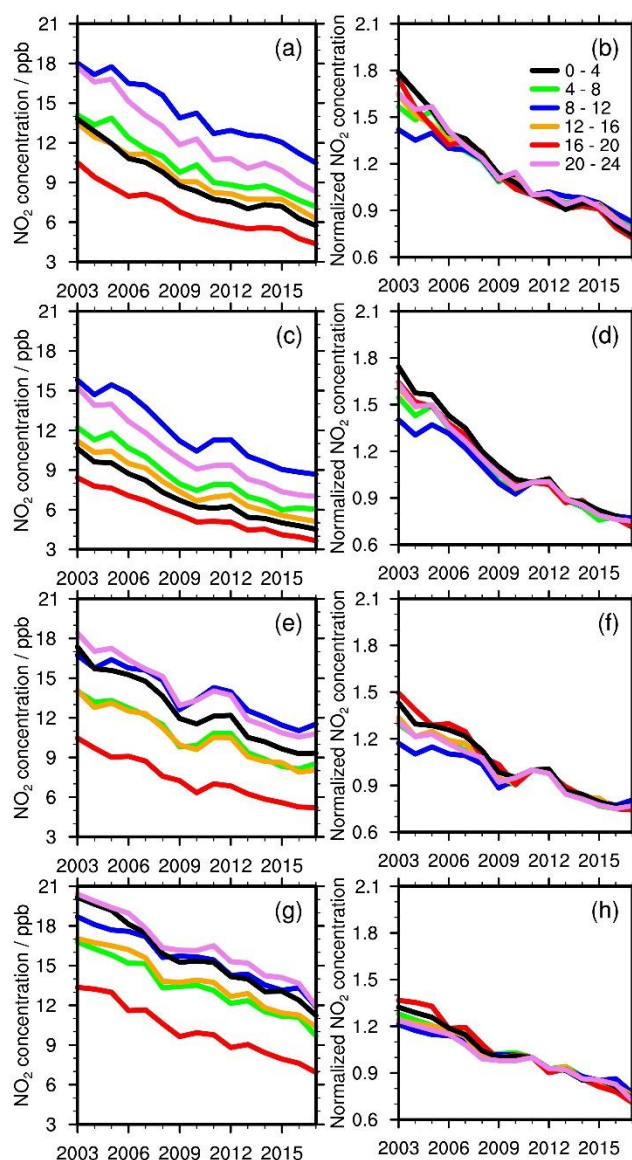
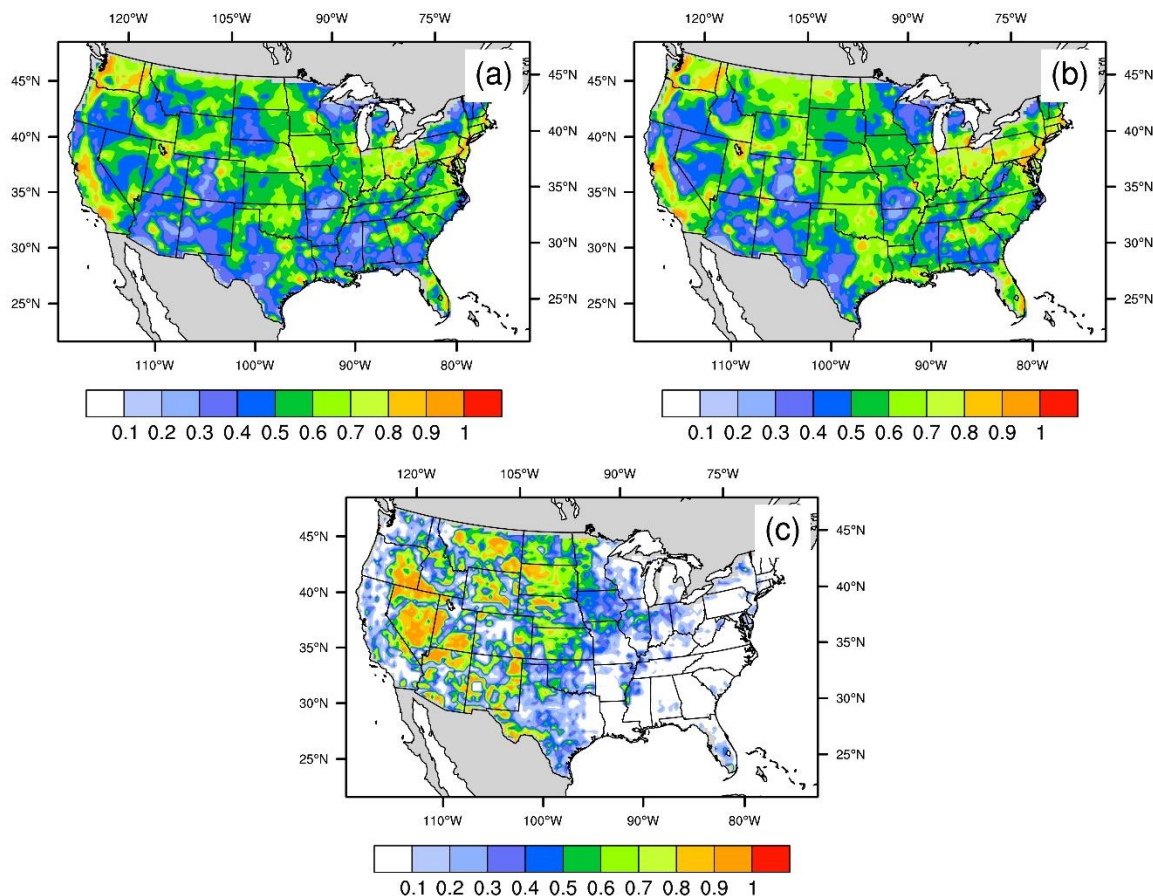


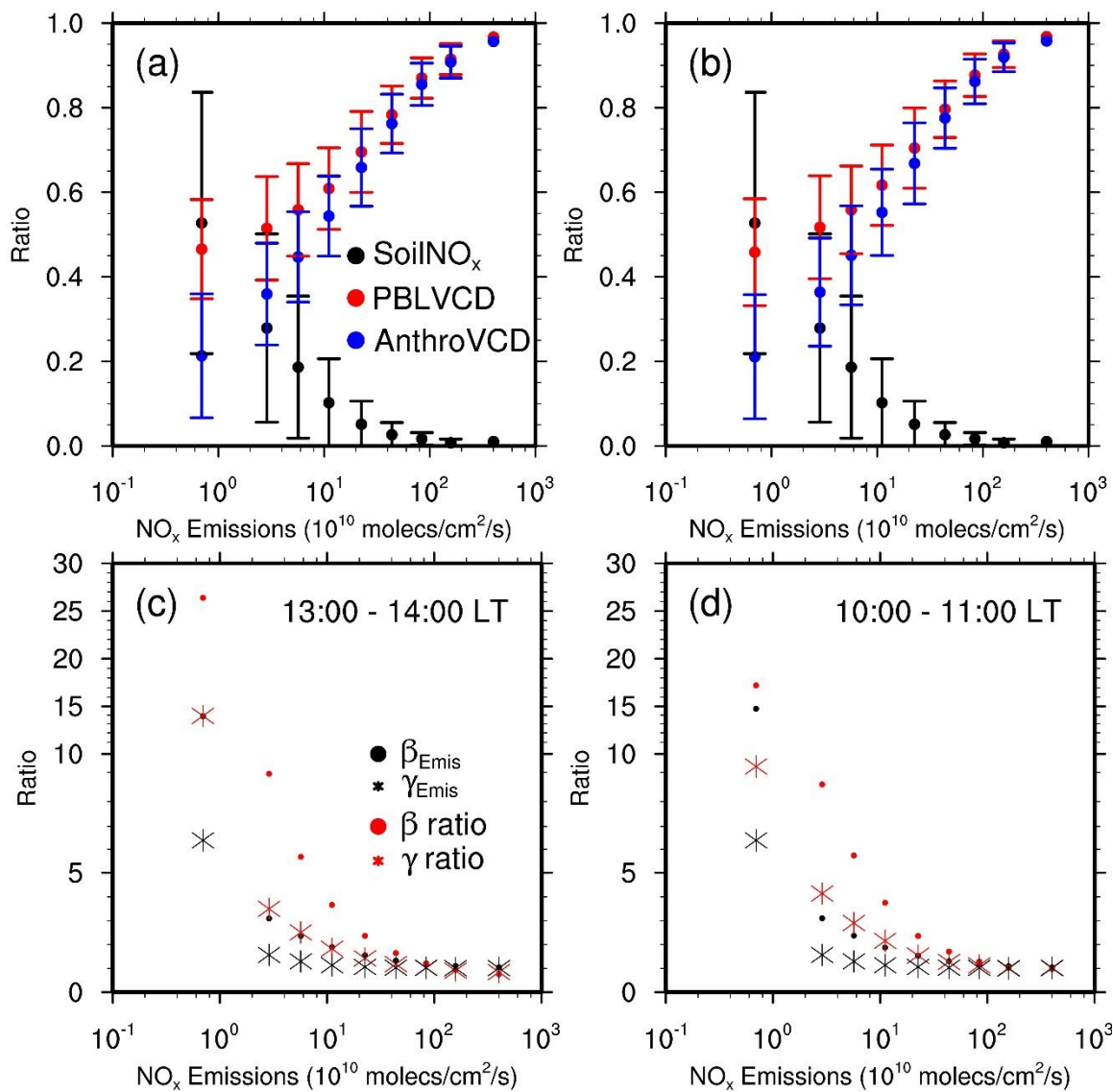
Figure S5. Annual variations of AQS NO₂ surface concentrations at different hours on weekdays in spring (a, b), summer (c, d), autumn (e, f), and winter (g, h). Left panels show absolute NO₂ concentrations, and right panels are their relative variations normalized to 2011. To conduct reliable and consistent comparisons, we only used monitoring sites satisfying the seasonal $RCI < 50\%$ and continuity criteria on weekdays from 2003 – 2017.



138

139 Figure S6. Distributions of (a) NO₂ TVCD fraction that is in the boundary layer (< 2810 m) at
 140 13:00 – 14:00, (b) NO₂ TVCD fraction in the boundary layer (< 1290 m) at 10:00 – 11:00, (c) the
 141 fraction of soil NO_x emissions in all surface sources (anthropogenic + soil) on weekdays for July
 142 2011. As the lifetime of NO₂ in the free troposphere (several days ~ 2 weeks) is much longer than
 143 that in the boundary layer (~ 10 hours), local lightning NO_x emissions cannot represent NO₂
 144 VCDs in the free troposphere. In this study, we apply NO₂ VCD in the free troposphere to
 145 analyze the impact of lightning NO_x on the nonlinear relationships between anthropogenic NO_x
 146 emissions and NO₂ TVCDs and use lightning NO_x and NO₂ VCD in the free troposphere
 147 interchangeably in the following.

148



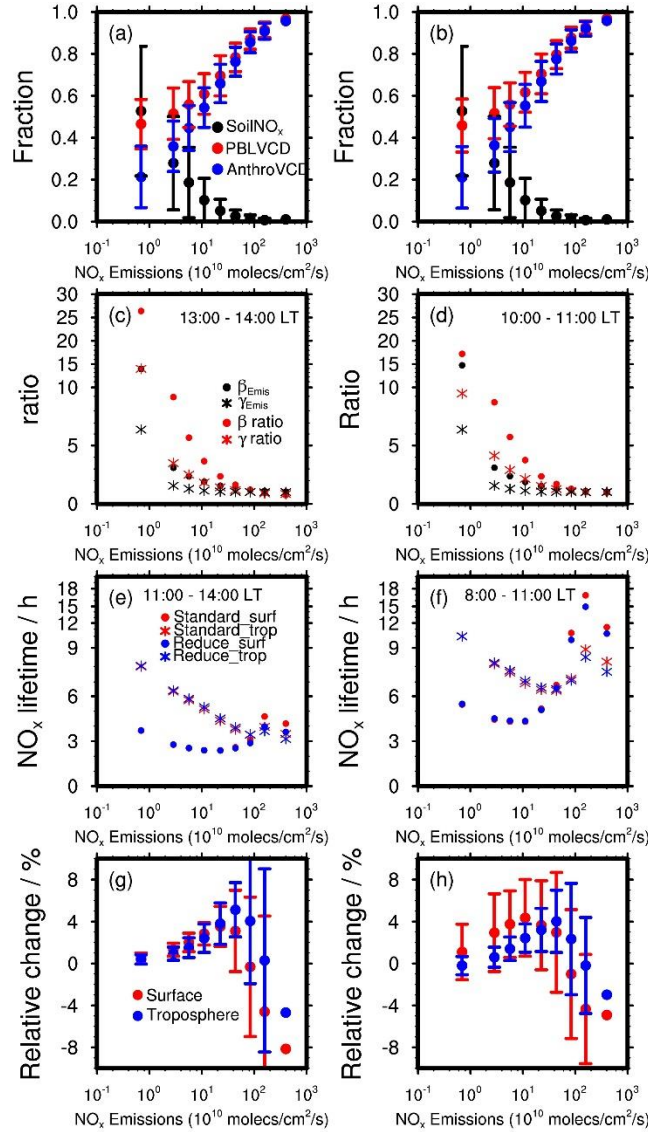


Figure S7. (a) Distributions of the fractions of surface NO_x emissions emitted by soil (“SoilNO_x”), the portions of NO_2 TVCDs in the boundary layer (“PBLVCD”), and the fractions of NO_2 TVCDs from anthropogenic NO_x emissions (“AnthroVCD”) as functions of NEI2011 anthropogenic NO_x emissions at 13:00 – 14:00 LT on weekdays for July 2011 over the CONUS.

The fraction of NO_2 TVCDs from anthropogenic NO_x emissions is equal to $\left(1 - \right.$

$$\left. \frac{E_{\text{soil}}}{E_{\text{soil}} + E_{\text{anthropogenic}}} \right) \times \left(\frac{\text{TVCD}_{\text{boundary}}}{\text{TVCD}_{\text{boundary}} + \text{TVCD}_{\text{free}}} \right), \text{ where } E_{\text{soil}} \text{ denotes soil } \text{NO}_x \text{ emissions,}$$

$E_{anthropogenic}$ denotes anthropogenic NO_x emissions, $TVCD_{boundary}$ denotes NO_2 TVCDs in the boundary layer, and $TVCD_{free}$ denotes NO_2 TVCDs in the free troposphere. The calculated data are grouped into 9 bins as in Figure 2. (b) Same as (a), but for 10:00 – 11:00 LT. (c) Distributions of β_{Emis} , γ_{Emis} , β , and γ as functions of anthropogenic NO_x emissions at 13:00 – 14:00 LT on weekdays for July 2011 over the CONUS. β and γ are the same as Figure 2. β_{Emis} and γ_{Emis} denote β and γ values when no other factors are taken into consideration except for soil NO_x emissions, anthropogenic NO_x emissions, and NO_2 in the free troposphere. $\beta_{Emis} =$

$$\frac{15\%}{15\% \times \left(\frac{E_{anthropogenic}}{E_{anthropogenic} + E_{soil}} \right) \left(\frac{TVCD_{boundary}}{TVCD_{boundary} + TVCD_{free}} \right)} = \left(\frac{E_{anthropogenic} + E_{soil}}{E_{anthropogenic}} \right) \left(\frac{TVCD_{boundary} + TVCD_{free}}{TVCD_{boundary}} \right),$$

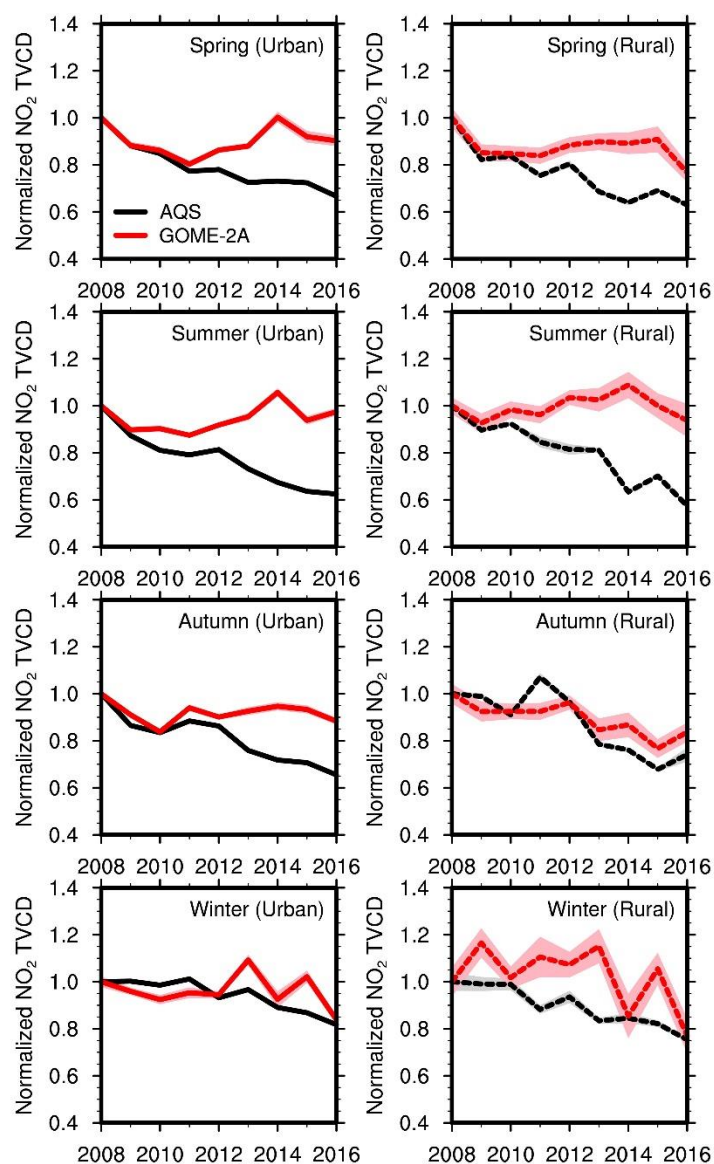
$$\text{and } \gamma_{Emis} = \frac{15\%}{15\% \times \left(\frac{E_{anthropogenic}}{E_{anthropogenic} + E_{soil}} \right)} = \left(\frac{E_{anthropogenic} + E_{soil}}{E_{anthropogenic}} \right). \text{ It is noteworthy that here we}$$

assume no interactions between the boundary layer and the free troposphere, boundary-layer NO_x are only related to soil and anthropogenic NO_x emissions, and lightning NO_x only affect NO_2 in the free troposphere. The assumptions are reasonable as the time scale (~ 1 week) of the interactions between the boundary layer and the free troposphere ~~are-is~~ much longer than NO_x lifetime in the boundary layer, and ~~in this study,~~ only a small fraction of lightning NO_x is distributed into the boundary layer in this study. Therefore, β_{Emis} and γ_{Emis} roughly represent the contributions of background sources (lightning NO_x and soil NO_x) to β and γ values. The differences between β (γ) and β_{Emis} (γ_{Emis}) indicate the contribution of non-emission factors to β (γ) values, such as chemistry, transport, NO_2 hydrolysis on aerosols, and dry ~~and wet~~ depositions. (d) Same as (c), but for 10:00 – 11:00 LT. From (c) and (d) this figure, we find that both background sources (lightning NO_x + soil NO_x) and non-emission factors are important when considering the nonlinear relationships among NO_x emissions, NO_2 surface concentrations, and NO_2 TVCDs in low-anthropogenic- NO_x emission regions. (e) Distribution of NO_x chemical lifetimes as functions of anthropogenic NO_x emissions at 11:00 – 14:00 LT on weekdays for July 2011 over the CONUS. “Standard_surf” denotes NO_x chemical lifetimes at the surface layer from

the standard REAM simulation (“group 1” in Section 3.1); “Standard_trop” denotes average NO_x chemical lifetimes in the troposphere for “group 1”; “Reduce_surf” denotes NO_x chemical lifetimes at the surface layer for “group 2” with anthropogenic NO_x emissions reduced by 15%; “Reduce_trop” denotes average NO_x chemical lifetimes in the troposphere for “group 2”. In this study, we used the lifetimes at 11:00 – 14:00 LT but not 13:00 – 14:00 LT to partly include the accumulation effect of NO_x emissions: NO₂ TVCD and NO₂ surface concentrations at 13:00 – 14:00 LT are not only affected by NO_x emissions at 13:00 – 14:00 LT but also by NO_x emissions before that due to the NO_x chemical lifetime of several hours in daytime. (f) Same as (e), but for 8:00 – 11:00 LT. (g) Relative changes of NO_x chemical lifetimes at 11:00 – 14:00 LT on weekdays for July 2011 over the CONUS due to the 15% decrease of anthropogenic NO_x emissions in “group 2”. “Surface” denotes the relative changes of NO_x chemical lifetimes at the surface, while “Troposphere” denotes the relative changes of average NO_x chemical lifetimes in the troposphere. We first calculated the relative changes in each grid cell via $\frac{lifetime_{Reduce}}{lifetime_{Standard}} - 1$, and then binned the calculated data into 9 groups as Figure 2. (h) Same as (g), but for 8:00 – 11:00 LT. In the chemical lifetime calculation, we included sinks from the reaction of OH + NO₂ and net losses due to organic nitrate production from the reactions of RO₂ with NO or NO₂ except for peroxyacyl nitrates (PANs), because PANs can be either a source or sink of NO_x depending on transport and chemistry. Only accounting for the sink from the reaction of OH + NO₂ produces significant different lifetimes in low-anthropogenic-NO_x emission bins and has less impact on high-anthropogenic-NO_x emission regions, which, however, does not affect our conclusions derived from subpanels (g) and (h) (the mean relative differences of chemical lifetimes between “group 1” and “group 2” are still < 10% in all bins); the chemical nonlinearity contributes little to β and γ values in low-anthropogenic-NO_x emission regions. Although not shown here, the impacts of NO₂ hydrolysis and NO₂ dry deposition on β and γ values are even smaller than those of chemical nonlinearity. Therefore, the differences between β (γ) and β_{Emis} (γ_{Emis}) in low-

206 anthropogenic-NO_x emission bins in (c) and (d) mainly indicate the contribution of transport to β
207 (γ) values. Error bars in (a), (b), (g), and (h) denote standard deviations.

208

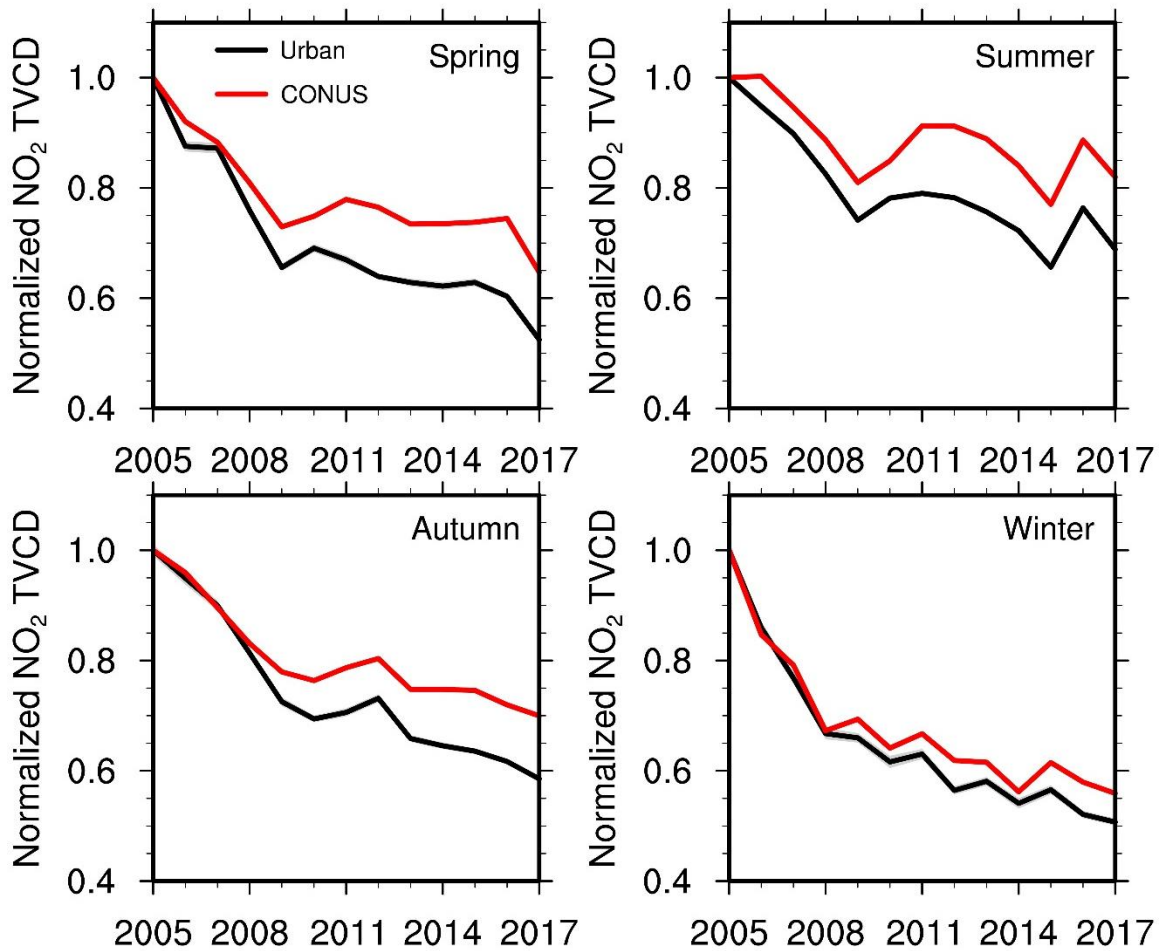


209

210 Figure S8. Same as Figure 4, but for AQS NO₂ surface concentrations and coincident GOME-2A

211 NO₂ TVCD data during 2008 – 2016.

212



213

214 Figure S9. Relative variations of OMI-QA4ECV NO₂ TVCD data for urban regions (black lines)
 215 and the whole CONUS (red lines) from 2005 – 2017 in 4 seasons.

216